5-2014

DENSITY FUNCTIONAL THEORY STUDY OF THE THERMODYNAMICS OF CATALYTIC REMEDIATION OF NITRATE IN WATER

Lizzie Bollmann
Clemson University, lbollma@clemson.edu

DENSITY FUNCTIONAL THEORY STUDY OF THE THERMODYNAMICS OF CATALYTIC REMEDIATION OF NITRATE IN WATER

A Thesis
Presented to
The Graduate School of
Clemson University

In Partial Fulfillment
of the Requirements for the Degree
Master of Science
Chemical Engineering

---

by
Lizzie Bollmann
May 2014

Accepted by:
Dr. Rachel B. Getman, Committee Chair
Dr. David Bruce
Dr. Elizabeth Carraway

ABSTRACT

Over 1 billion people worldwide lack access to safe drinking water and 5,000 people die each day due to drinking contaminated water[1]. With the development of new industries, new substances and chemicals are entering the waters every day, and the current water treatment processes are unable to remove them entirely. For example, agriculture is the world's heaviest consumer of water, and nitrates and nitrites from fertilizers are washed away with the water to rivers and streams[2]. These chemicals can cause problems to humans and to the environment. To humans, they can cause methemoglobinemia, also known as "blue baby syndrome". To the environment, they can cause eutrophication, a phenomenon greatly reduced the dissolved oxygen content of the water harming the aquatic animals.

Catalytic remediation of water is a promising strategy to meet the ecological, social and economic demands of the future, [3] but the high-cost of developing new catalysts for wastewater treatment applications often limits their adoption in new wastewater treatment processes. [4]

In this work, we investigate nitrate and nitrite reduction over spherically shaped gold-based catalysts. Starting with Au_{13} we can modify composition by replacing just one or two atoms with other metals, forming $Au_{12}X$ and $Au_{11}XY$ clusters. Here, X/Y = Fe, Pd, In, and Cu, which were chosen because they cover a large range of groups in the periodic table, are relatively inexpensive, and are non-toxic. All of the tested catalysts

tested show favorable behavior for nitrate reduction but not for nitrite reduction. We find that X,Y = Fe, Pd show the best results for nitrite dissociation because of the exothermic behavior towards both reactions. We also compute ammonia and water dissociation energies on the catalyst surfaces to determine if the catalysts will dissociate these species.

This work provides the essential framework for modeling pollutant remediation in water. The methods described in this thesis were used to screen a range of catalysts compositions and identify small group of catalysts that performs the desired reactions selectively over water and organic matter.

DEDICATION

To my daughter and best friend, Alexandra Alfaro, for being my driving force and motivation in life.

ACKNOWLEDGMENTS

First, I would like to thank the Obermann Center for Advanced Studies, the University of Iowa and Clemson University for funding this project. I would also like to thank the Palmetto Cluster for computational resources.

Next, I would like to thank my committee, Dr. Rachel Getman, Dr. David Bruce and Dr. Elizabeth Carraway for their help and suggestions to improve my project and research. I would especially like to express my deepest gratitude to my advisor Dr. Rachel Getman, for being an excellent guide and teacher and for her unconditional patience, help and advice every time I needed it.

Also a big thank you to my colleague and friends: Anu, Felipe, Cameron, Kryssia and Nikki, for your friendship and for making everyday so much fun.

At last, I would like to thank my family: My parents, my husband and my daughter, for your support, patience and love through this process. I would not be here if it wasn't for you.

TABLE OF CONTENTS

Table of Contents (Continued)

LIST OF TABLES

LIST OF FIGURES

CHAPTER ONE
MOTIVATION

1.1 Water

Water covers two thirds of the world's surface and is essential to all forms of life. People all over the planet are dependent on water, and water provides habitat for fresh and salt-water animals and plants. The Food and Agriculture Organization of the United Nations states that less than 1 percent of water on earth is available for human use. [1] Usually, we obtain our tap water from surface water (rivers, lakes, streams) or ground water (found beneath the earth's surface). After the water has been used in homes, industries, and business, it is considered wastewater. Wastewater also contains sewage and storm runoff. Both tap water and wastewater need to be treated to reduce chemical pollutants and pathogens.[2]

1.1.1 Water pollution

While population and demand on freshwater resources are increasing, supply will always remain constant. [5] Present water consumption is 80-100 gallons of water per person per day. [6] On the other hand, every day, 2 million tons of treated sewage and industrial and agricultural waste are discharged back into the water supply. [6]

In the last couple of years, changes in industrial processes, technological developments, changes in land use, business innovations, and many other factors have affected the amount and complexity of industrial wastes, challenging traditional treatment technologies. [7] The general population also contributes to the growing concentrations of water pollution with the substances that get dumped down our drains, such as personal

care products, which can be harmful to humans and animals. [8-10]

1.1.2 Nature and types of water pollutants

There are currently 83 different kinds of potentially harmful pollutants in water that are regulated by the EPA. [11] Water pollutants can be any chemical, biological, or physical materials that degrade the water quality. [12] The most usual types of pollutants are petroleum products, pesticides and herbicides, heavy metals, hazardous waste, sediment, infectious organisms, thermal pollution, and excess organic matter. [13] They can be classified depending on their source or depending on the hazards they present.

1.1.3 Point vs. Nonpoint sources

Water pollutants can come from two types of sources: point and nonpoint sources. When the pollution comes from a single source, like a factory or sewage, and is dumped into a water body through a single pipe, is called a point source of pollution. [14] In this case, the pollutants need to be treated before being discharged into a water body. If the discharges from point sources are not treated properly, they can result in water pollution and unsafe water.

Diffuse sources of pollution like land runoff, precipitation, atmospheric deposition, drainage, seepage or hydrologic modification are called nonpoint sources of pollution. [14] The concentration and type of nonpoint pollutants varies from place to place and may not always be fully assessed, which makes it difficult to treat them successfully.[15]

1.1.4 Water and Wastewater treatment

The remediation of water, whether it's tap water or wastewater, will usually focus on improving the physical, chemical and biological characteristics of the water, by performing a set of unit operations. [16] (See Figure 1.1 and 1.2.) Each unit operation is designed to deal with broad classes of pollutants in order to improve parameters like color, taste, odor, turbidity and to remove general chemical constituents like toxic organics and inorganics. [16] A traditional water treatment plant includes a rapid mixing tank, which carries out coagulation, flocculation, sedimentation, filtering, and disinfection. [12] In a wastewater treatment plant there is a pretreatment stage where grit, fat and grease are removed. [16] Then a primary treatment takes place in a primary clarifier, in which the sludge settled and the water are separated. Later, the water goes through a secondary treatment process in which the water is treated biologically to further remove the pollutants in the system. In this case, different types of bacteria further reduce pollutants such as ammonia and nitrate. The activated sludge containing the bacteria and the clear water are separated. At last, the water goes through disinfections to remove the pathogens. The traditional methods for water and wastewater treatment are usually pretty efficient; the problem is that there are specific constituents that cannot always be removed by the traditional methods.

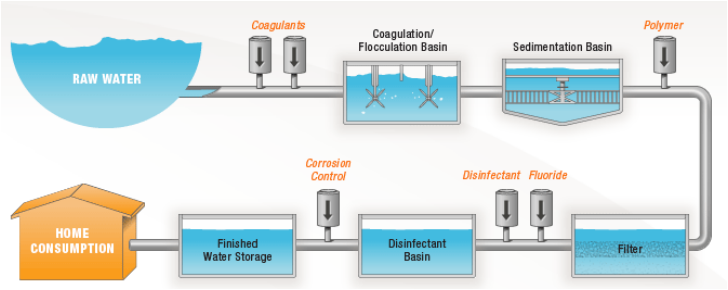

Figure 1.1 Simplified process flow diagram for a typical water purification plant. Reproduced from Ref. 17 © Copyright by Denver Water 2014

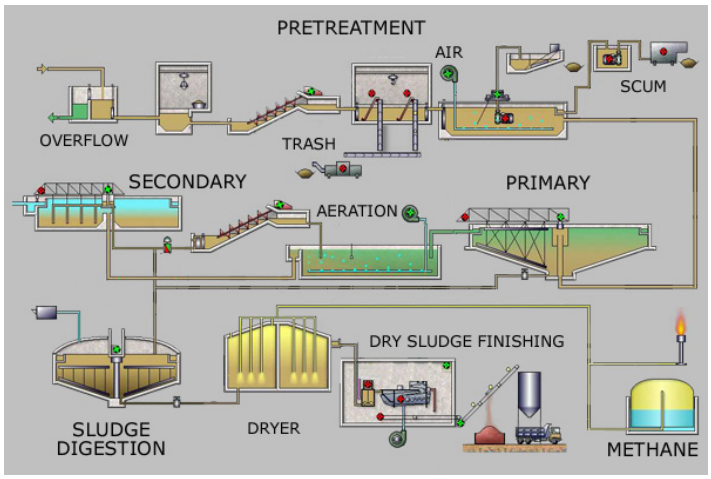

Figure 1.2 Simplified process flow diagram for a typical large-sale wastewater treatment plant. Reproduced from Ref. 18

Sometimes, the removal of particular pollutants, for example pharmaceuticals and personal care products (PPCP) [19], cannot be made with the traditional methods and there is a need of remediation with more advanced techniques. [19] This can be in done different ways, depending on the nature of the pollutant and the amount. This can be accomplished by membrane filtration and separation, reverse osmosis, ion exchange, activated carbon or different physical/chemical treatments. [12] For example hydrophobic acids, which are

emerging pollutants present in natural organic matter, are removed using advanced oxidation processes (AOPs) such as UV or O_3 treatment. [20]

1.2 Nitrates

1.2.1 Sources

Agriculture is the world's heaviest consumer of water and the fertilizers are washed away with the water to rivers and streams. Nitrate, which is typically found in fertilizers, is a persistent contaminant and the most common contaminant in the world's groundwater aquifers. [21] Nitrate concentration has increased by an estimated 36% in global waters since 1990. [22] Leakage from septic tanks, sewage, and erosion of natural deposits are also sources of nitrates.

1.2.2 Effects

High nitrate levels can harm humans and the environment. To humans, consumption can cause methemoglobinemia, or blue baby syndrome, a condition found especially in infants less than six months old. [23] When a person has this condition, methemoglobin (a form of Hemoglobin) is produced in excess. Hemoglobin is the molecule in red blood cells that distributes oxygen to the body. Methemoglobin cannot release oxygen so it cannot be delivered effectively to body tissues. [24]

In the environment, high levels of nutrients (nitrates, phosphates) cause eutrophication. Eutrophication is the process when a high concentration of nutrients is found in water. Eutrophication stimulates an explosive growth of algae. When the algae

dies and is decomposed by microorganisms, it depletes the water of oxygen. This causes the death of other aquatic organisms, such as fish. [25] Such waters may become hypoxic (oxygen poor) or anoxic (completely depleted of oxygen). In the northern part of the Gulf of Mexico, there's a dead zone of 17,000 km.^{2} Nutrient runoff from the Mississippi river is the main nutrient source that depleted the oxygen. [26]

1.2.3 Removal

Several different strategies have been implemented for nitrate remediation. Physicochemical processes, biological decomposition, and electrochemical reduction of nitrates are some of the most common methods studied. [4,27-41]

For the drinking water industries, ion exchange resins containing base anions, usually chloride or sodium bicarbonate, have been used. [16] The water is passed through the resin bed and nitrate ions are exchanged for the anions until the capacity is exhausted. Afterwards, the resin needs to be regenerated by using a concentrated solution of sodium chloride or sodium bicarbonate. The regeneration costs are expensive. [42] Over a 20-year plant life, the regeneration of the resin costs can be more than double than the initial equipment cost. [27] While this method has proven to be effective, it does not eliminate nitrates completely. [42] Eliassen, et al. reported a nitrate reduction from 18 to 6.8 mg NO_3^-/L[41], and Philipot reported nitrate reduction from 15.8 to 5.7 mg NO_3^-/L. [43]

Biological reduction of nitrates to nitrogen is a common way to reduce nitrates in wastewater. Under very specific conditions and in the absence of oxygen, some microorganisms can use nitrate as their oxygen source. [16] The process is called anoxic

denitrification, and the end products from denitrification are N_2, CO_2, H_2O and new cell material. In most wastewater treatment plants this process is divided into two steps. First, in an aerobic tank, ammonia is oxidized to nitrite and then to nitrate, and then in an anoxic tank, the nitrate is reduced. These processes can be done different ways. In the suspended growth, microorganisms are suspended in the water and in the attached growth, microorganisms grow on a solid surface. [16] The problem with these methods is that there are very specific conditions that need to be maintained always[42] and the process can take up to 20 days. [12] Conditions that affect the efficiency of denitrification include nitrate concentration, anoxic conditions, presence of organic matter, pH, temperature, alkalinity and the effects of trace metals. [44]

Another method for nitrate remediation used in the drinking water industry is catalytic reduction. A catalyst is a substance that alters the rate of a chemical reaction by providing an alternate reaction pathway and lowering the activation energy without being consumed. [45] As far as we know, catalysis has been used for many millennia to produce alcohol by fermentation, but the first known reference to the use of inorganic catalysis is from 1552, when Valerius Cordus used sulfuric acid to catalyze the conversion of alcohol to ether. [46] Since then, catalysis has gained importance, and now almost every industrial reaction involves a catalyst in some part of the process. [20,47] Catalytic reduction for nitrate removal was studied by Hörold et al. at the end of the 1980s as an alternative to decrease nitrate concentration in drinking water. [29] They reported that in the presence of hydrogen, catalysts comprised of palladium and alumina removed nitrate with 98% effectiveness, while lead/copper on alumina removed 100 mg NO_3^-/L with high effectiveness in less

than an hour. This was a big breakthrough because it increased the activity over 30 times compared to biological denitrification. Since then, several modified noble metal catalysts have been tested for nitrate reduction. [4,27-31,33,35-37,39]

Nitrates are usually selectively converted to nitrogen over a solid catalyst by adding hydrogen. This can be represented by the overall reaction

$$2NO_3^- + 5H_2 \rightarrow 4H_2O + N_2 + 2OH^- \qquad \text{Equation 1}$$

Among the catalysts tested, those based on palladium (Pd–Cu, Pd–Sn, Pd–In and Pd–Zn) showed the most favorable results. [32,33] As far as catalytic nitrate reduction is concerned, the changes in activity and selectivity resulting from alloying of the metals are still not completely understood.

CHAPTER TWO
METHODS AND METHODOLOGY

2.1 Methods

In this work we use quantum mechanic simulations to study the catalytic reduction of nitrate in water. Gold-based nanoparticles are used as catalysts and a solvation model is used to include the water surroundings of the reaction.

2.1.1 Computational catalysis

With the help of computers and theoretical methods, many major catalytic properties can be calculated using computational catalysis. Many important reaction properties, like transition states and activation energies, are difficult to quantify experimentally. Theoretical methods have become more and more accurate in the recent past, [48] making it possible to understand chemical processes and the manipulation of the material structure.

2.1.2 Reaction energetics of a catalyzed reaction

In most reactions, there is a series of elementary steps that lead from reactants to products, and a small subset of these are usually slower than the rest. These steps are usually called the rate-limiting steps. Usually, the steps that qualify as rate limiting depend on the energy barriers, which reactants must overcome in the course of their transformation to products. [49]

When a reaction is catalyzed, it proceeds in a new and more energetically favored pathway. The elementary steps involved in the reaction will change and therefore the

activation energy will change as well.[49] The rate expression, which is a function of the temperature and the concentrations of reactants, can be given by

$$r = k * C^n \qquad \text{Equation 2}$$

Where k is the rate coefficient, C is the concentration of a species and n is the order of the reaction. The rate constant k varies with absolute temperature according to the Arrhenius equation:

$$k = A \exp(- E_a / R\,T) \qquad \text{Equation 3}$$

where A is the pre-exponential factor, as also known as a frequency factor. It represents the frequency of collisions between reactant molecules. E_a is the activation energy, R is the ideal gas constant, and T is the absolute temperature. The catalyst can act to lower the activation energy and thus influence the rate of the reaction. This can be better described in a potential energy plot, such as the one in Figure 2.1. In this figure, the green line shows the potential energy of reactants becoming products in an exothermic, uncatalyzed reaction. The reactants have to go to a high-energy state, the transition state, and cross an energy barrier equivalent to the activation energy before becoming products. The higher the activation energy, the harder it is for a reaction to take place.

The red line represents the same exothermic reaction using a catalyst. The catalyst hasn't affected the reactants or products, but it does affect the reaction pathway, the activated complex, and the activation energy.

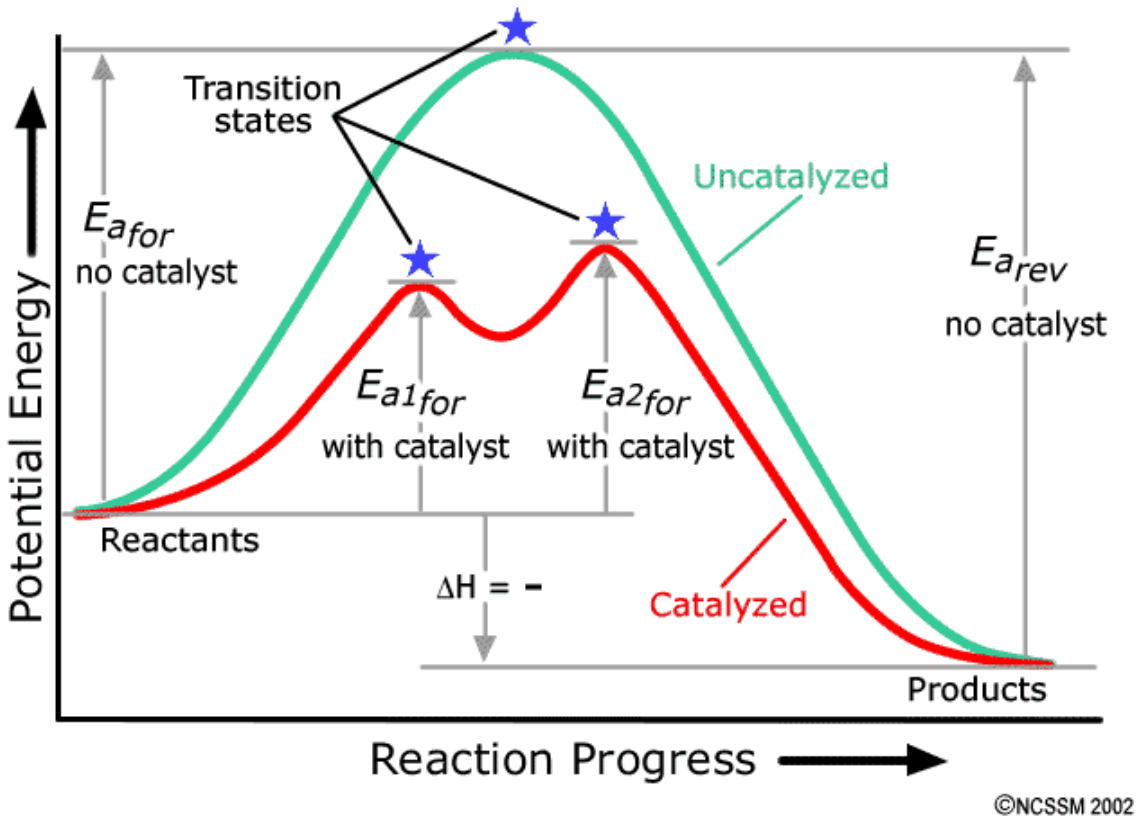

Figure 2.1 Generic diagram of an exothermic reaction with and without the presence of a catalyst. Reproduced from Ref. 50 ©NCSSM 2002

2.1.2.1 Types of catalysts

A catalyst can be classified as homogeneous or heterogeneous. For example, if a catalyst is dissolved in a liquid reaction medium, and so are the reactants and products, it's called a homogeneous catalyst, since the catalyst and the reactants and products are in the same phase of matter. But if it is a multiphase system in which the catalyst is in one phase and the reactants and products are in another, e.g., a solid catalyst in a medium comprising liquid and/or gas phase reactants and products, it is called heterogeneous catalyst. [48]

2.1.2.2 Adsorption and adsorption sites

Adsorption is a necessary step in catalytic reactions. This step involves a molecule in the gas phase or in solution binding to atoms of the solid catalyst. Adsorption energies can be calculated using:

$$E_{adsorption} = E^{adsorbate} - (E^{molecule} + E^{clean\ catalyst}) \qquad \text{Equation 4}$$

where the first term on the RHS is the electronic energy of the adsorbate-catalyst system and the terms in parentheses are the sum of electronic energies of the isolated gas phase molecule ($E^{molecule}$) and the clean catalyst ($E^{clean\ catalyst}$).

Once the molecule is bound to the catalyst it's called an adsorbate. Adsorbates can bind to a catalyst surface in different positions and sites. Depending on the number of catalyst atoms that are in direct contact with the adsorbate, we tend to classify the sites as onefold, twofold, or threefold sites. For example, when an adsorbate binds to a catalyst in a twofold site, it forms bonds with two catalyst atoms. Determining the types of adsorption sites where adsorbates prefer to bind is a necessary step in computing catalytic phenomena. Appendix 1 summarizes the adsorption energies and most favorable adsorption sites for all the NO_x species involved in this work.

2.1.2.3 Reaction mechanism

A reaction usually takes place in several steps. The mechanism for a reaction is the sequence of all the elementary reactions (or steps) that describe how the overall reaction proceeds. These elementary reactions express how molecules or ions react with each other and usually proceed at various speeds.[51] The slowest step is the rate-

determining step of the overall reaction, and the reaction rate (the one which would be the most likely to be observed experimentally) is controlled by the rate of the slowest step. [45]

2.1.2.4 Selectivity

Once species have adsorbed to the catalyst surface, they may continue to react to form the desired products or other species. This will lead to the formation of desired and undesired products. This may happen in different ways. There may only be one reactant present in the reaction, but this reactant can be converted in two different ways that will lead to two products. Also, if the reaction mixture contains two or more reactant molecules, one may be converted faster than the others. [48] The ability of catalysts to direct a reaction to yield particular products is called selectivity.[45] The selectivity of a catalyst strongly depends on its adsorption properties, since it is in this step and during the following dissociation, that the reactants are activated for the catalytic reaction. [45]

2.1.2.5 Poisoning

A catalyst can adsorb different molecules and atoms present in the reaction environment. If the adsorbed species are very stable and a very exothermic adsorption takes place, it prevents further adsorption of other species, and a substantial loss in activity takes place. [48] This phenomenon is known as catalyst poisoning.

2.1.2.6 The Sabatier Principle

Thus a balance is needed in how strongly a species binds to a catalyst. As P. Sabatier stated it in 1922, during the course of heterogeneous catalysis, the interactions between the catalyst and the intermediate substances needed to be stable enough to be

formed on the catalyst surface, but unstable enough to decompose and yield to final products.[52] This was defined as the "optimum strength of bonding" and is known as the Sabatier principle.

2.1.3 Quantum Mechanics

In computational catalysis, we can provide insight into how well a catalyst will work for a particular reaction by calculating such quantities as adsorption energies and activation barriers. We do this using quantum mechanics, as bond breaking and forming processes are quantum chemical by nature. At the heart of quantum mechanics is the multi-body wavefunction.[53]

$$\Psi(r_1, r_2, r_3, \ldots, t) \qquad \text{Equation 5}$$

Here, $r_1, r_2, r_3, \ldots$, etc. are the position vectors of all fundamental particles in the system in time t. When we perform a quantum chemical calculation, the fundamental particles are the electrons.

The wavefunction is determined by the Schrödinger equation, the quantum-mechanical analogy of Newton's equations of motion. For a single particle traveling in a potential energy field, Schrödinger's equation reads.[53]

$$i\hbar\frac{\partial}{\partial t}\Psi(r,t) = \left[-\frac{\hbar^2}{2m}\nabla^2 + V(r,t)\right]\Psi(r,t) \qquad \text{Equation 6}$$

where

$\hbar = h/2\pi$, where h is Planck's constant = $6.62606957 \times 10^{-34}$ m^2 kg / s;

m is the mass of the particle;

∇^2 is the Laplacian operator, and the term $\frac{\hbar^2}{2m}\ \nabla^2$ is the kinetic energy;

V (r, t) is the potential energy function.

To solve it, a separation of variables technique can be used, where we write the wavefunction as the product of a spatially dependent function and a time-dependent function. [54]

$$\Psi(r,t)=\psi\,(r)\varphi(t) \qquad \text{Equation 7}$$

This yields to the time independent Schrodinger equation

$$E\psi(r) = [-\frac{\hbar^2}{2m}\ \nabla^2 + V(r)]\psi(r) \qquad \text{Equation 8}$$

Where $-\frac{\hbar^2}{2m}\ \nabla^2 + V(r)$ is the Hamiltonian operator H, and E is the energy of the state ψ.

We can rewrite this

$$E\ \psi\ (r) = H\ \psi\ (r) \qquad \text{Equation 9}$$

which is the most recognizable form of the time independent Schrödinger equation. [54]

2.1.3.1 Density Functional Theory

One approach for determining electronic structure is the density functional theory (DFT) of Hohenberg, Kohn, and Sham.CITE Instead of computing the multidimensional

wavefunction, density functional theory is concerned with computing only the electron density ρ(r), which gives us a measure of the probability of an electron being present at a specific location. [53]

In DFT, the ground state energy state is written as[55-58]

$$E\,\rho(r) = \int V(r)\,\rho(r)dr + E_{KE}[\rho(r)] + E_{H}[\rho(r)] + E_{XC}[\rho(r)] \qquad \text{Equation 10}$$

The first term on the RHS gives the potential of the electrons due to the nuclei in the system, the second term is the kinetic energy functional, third term is the electron-electron repulsion functional, and the last term is the exchange-correlation functional. A functional is a function of another function, in this case, referring to functions of the electron density.

2.1.3.2 Exchange Correlation Functional

This functional is not exactly known, but there are many approximations to solve it. These methods include the Local Density Approximation (LDA) [59], the Gradient Expansion Approximation (GEA), and the Generalized Gradient Approximation (GGA) and combinations of these.

In LDA, $E_{XC}[\rho(r)]$ depends only on the value of electron density at each point in space, [59] so it fails in situations where the density undergoes rapid changes. [60] In GGA both the electron density and the gradient of the density are taken into account. Among the most popular functionals today are two generalized gradient approximations, PW91[61] and PBE[62], of Perdew and coworkers.

2.1.3.3 Planewave approximation

The electrons in periodic systems can be described using planewaves instead of orbitals, as planewaves lend themselves better to periodic calculations. When a planewave approximation is used, the system to be modeled is assumed to be inside a unit cell that repeats itself infinitely in three dimensional space, creating periodic boundary conditions[63]. Instead of "orbitals," the energies and occupancies of "bands" are calculated. The bands are the ranges of energy that electrons can have in solids. The planewave is usually truncated at a specific cutoff energy, meaning that only bands with energies lower than that energy are taken into account. [64]

2.1.3.4 The pseudopotential approximation

Though DFT uses fewer computational resources than its multidimensional wavefunction counterpart, it still requires significant computational time. To save time, many methods use a "pseudopotential" approximation. This is approximation is based upon the knowledge that the core electrons do not normally participate in chemical bonding. Also, the core electrons are difficult to represent computationally due to their strong nuclear Coulombic potential. [65] Therefore, we can replace the core electrons with a pseudopotential, which is a simplified ionic core that interacts with the valence electrons in a computationally efficient manner. The valence electrons are explicitly taken into account in the calculations because they are the ones involved in the bond formation and bond breaking.

2.1.3.5 Electronic optimizations

In an electronic optimization, the ground state electron density is found at a specific arrangement of nuclei. It is also known as single point energy because the electronic energy of the system is found at a single geometry. The atoms are "fixed" in a position and only the electron density and the associated electronic energy are obtained. [66]

2.1.3.6 Geometry optimizations,

In a geometry optimization, the system goes through several configurations of the atoms to find a stable (local or global energy minimum) configuration of a molecule. In each geometrical step, an electronic optimization takes place. [66] The geometry optimizations can be driven by different factors, such as forces on the nuclei and stress tensors, and different mathematic algorithms can be used to determine the next position of the atoms involved. These usually contain information about the gradient and/or Hessian in the electronic structure.

2.1.3.7 Solvation Effects

When a reaction takes place in a solution, the solvent will interact with the system. These interactions, called solvation effects, need to be taken into account. These could be done explicitly, in which each molecule of the solvent is taken into account, but then the computational cost, meaning the computational resources and time used for the calculations, can become prohibitively large. [67] Therefore, there are solvation models to implicitly take into account the solvent as a continuous medium. This approximation makes it simple and inexpensive to calculate the solvation effects. In this work, the

Polarizable Continuum Model (PCM) was used. [68] This model calculates the free energy of solvation by generating a continuous and homogeneous dielectric field and creating a vacuum cavity to place the system to be modeled. PCM then calculates the electrostatic contributions, dispersion-repulsion interactions, and cavitation energy of the system in the presence of the dielectric field.

2.1.4 Catalytic Descriptors

For screening catalytic materials with the aid of computers, it is useful to determine trends for different catalysts across the periodic table[69]. These trends can be represented by one or more simple descriptors. A descriptor is an energy or property inherent to the catalyst that can be correlated to a thermodynamic or kinetic quantity of the reaction as it is being carried out on that catalyst. For example, adsorption energies can often be correlated to activation energies and thus are commonly used as descriptors of catalytic activity. A descriptor could be any intrinsic quantity of the catalyst that allows us to make predictions and describe the trends across different catalytic materials. [70] In most of the cases, there is more than one set of descriptors and all of them might be equally viable. [70] Identifying these descriptors is a primary challenge of computational catalysis. A descriptor has the function of describing or identifying important properties for classes of catalysts across the periodic table.

By using descriptors and correlating them to material properties we can significantly reduce screening time and cost to search for good catalysts for a specific

reaction, which could lead to catalytic remediation of water becoming an effective method to use.

2.1.4.1 D band correlations

Another common descriptor for metal catalysts is the d band, which represents the valence d orbitals. These bands are often used to described different properties of the solid such as electrical resistivity and optical adsorption. [71] In catalysis, the chemical reactivity of a metal catalyst can be described in terms of the d band model, which was popularized by Hammer and Norskov. [72] The chief principle underlying the model is that the binding energy of an adsorbate to a metal catalyst is largely dependent on the electronic structure of the material itself. The d band of a transition metal reacts with the molecular orbitals of the adsorbates. This interaction produces bonding and anti-bonding states. Additionally, the d band shifts up or down in energy[73] (see Fig 2.2). Metals with a higher d band center tend to bind adsorbates more strongly than metals with lower d band center[71-73], because the higher the d states are in energy relative to the Fermi level, which is the energy of the highest-energy occupied band, the higher in energy the anti-bonding states are, and therefore they are less likely to become filled. In a weak chemisorbption, there will be more filled up anti-bonding states located below the Fermi level[70]. In a stronger bond, more anti-bonding states will be high in energy and above the Fermi level.[70]

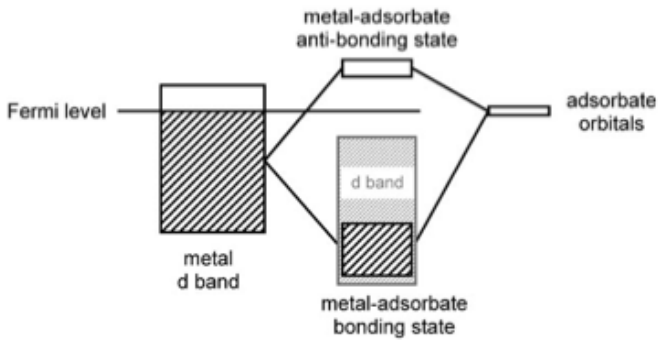

Figure 2.2 Simplified scheme describing the interaction of adsorbate orbitals with the d band metal. Shaded regions represent filled bands, and white regions represent unfilled bands. Reproduced from Ref. 74 with permission from the PCCP Owner Societies.

Most of the related articles in the literature, whether it's pure metal or alloys, focus on d band center relating to adsorption energies and how this can later be applied to estimate the activation energy of a reaction. [40,69,72,73,75]

2.1.4.2 Bader Charge Analysis

Another useful descriptor that we identified in this work is the partial charges that result on the different catalyst and adsorbate atoms due to adsorption. One of the outputs from a quantum mechanical DFT calculation is the electronic charge density, which can be partitioned in order to assign partial charges to different atoms. Richard Bader developed a way to define atoms in a system. [76] His definition of an atom is based on the electronic charge density. Typically in molecular systems, the charge density reaches a minimum between atoms, and this is a natural place to separate atoms from each other. [76] This is called the zero flux surface. The Henkelman group developed a computational method for partitioning a charge density grid into Bader volumes. [76-78] This is useful, to not only get the charge for each atom or molecule within a system, but to compute dipole

moments and bond strengths as well.

2.2 Methodology

In this work, we investigate the thermodynamics of nitrate and nitrite reduction

$$NO_3^- \rightarrow NO_2^- + O \qquad \text{Equation 11}$$

$$NO_2^- \rightarrow NO^- + O \qquad \text{Equation 12}$$

over spherically shaped gold-based catalysts in order to screen different catalysts for activity toward decomposing nitrates in water. Bulk gold is a noble metal, but nanosized gold has proven to be an effective catalyst for many reactions. [79-83] There have been studies to show that nanosize gold is non toxic[84], and because it is relatively inactive, it allows us to tune composition very carefully to maximize selectivity.

Catalysts were modeled using 13-atom icosahedral metal clusters (Figure 2.1) with 7Å diameters (1 Å = 10^{-10} m). [85] The geometries were obtained by cleaving a spherically shaped particle from the structure of bulk Au, which we obtained from the Pearson database[86], and performing a geometry optimization of the structure. Bulk Au is a face centered cubic (FCC) metal, meaning that, if we consider a small unit cell shaped like a cube, it has atoms located at each of the corners and in the centers of all the faces. The 13-atom icosahedral structure is convenient for screening because it is computationally efficient, and it comprises a large number of coordinatively unsaturated sites where molecules can adsorb, which we know is needed for Au-based catalysts, since bulk Au is inactive. Thirteen atoms is the smallest of the "magic" number of atoms you

can have in a nanoparticle, meaning the most favorable structures in nanoparticles. The next ones are 19 and 38 atoms. [87,88] On the other hand, the next icosahedral structure with these characteristics has 55 atoms, which is not computationally efficient. In reality, the Au_{13} icosahedron is likely not a realistic shape[79]; however, it provides a useful, and hopefully meaningful model that is computationally efficient and thus ideal for screening.

When adsorbates were included on the catalyst models, their geometries were fully relaxed, but the metal atoms were held fixed in order to preserve the icosahedral shape (see Fig. 2.3). We performed geometry optimizations for all adsorbates in the onefold, twofold, and threefold adsorption sites on our Au_{13} models and used the most favorable sites, i.e., those with the largest (most negative) adsorption energies, on all the other cluster compositions. Adsorption energies were calculated as presented in equation 3.

$$E_{adsorption} = E^{adsorbate} - (E^{molecule} + E^{clean\ catalyst}) \qquad \text{Equation 3}$$

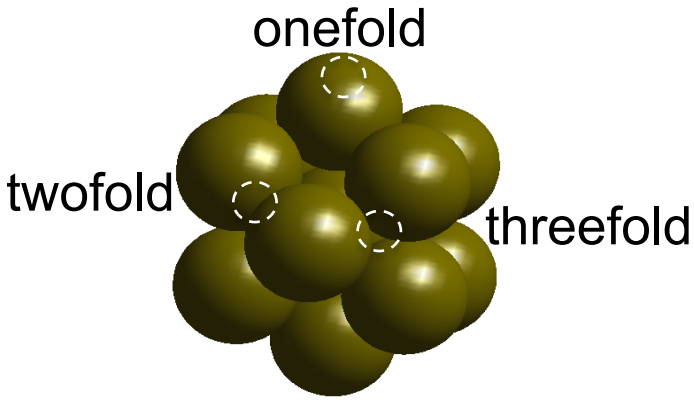

Figure 2.3 13-atom icosahedral Au nanoparticle showing high symmetry adsorption sites.

The catalyst composition was altered by replacing one atom in the Au_{13} cluster with another metal atom to form $Au_{12}X$ clusters (X = In, Cu, Pd, Fe). In, Cu, Pd, and Fe were chosen because they are relatively inexpensive, relatively non-toxic, and widely spread in the periodic table (See appendix B for a more detailed description about how we chose these metals). This allowed us to screen with different electronic structures and try to find trends across the periodic table.

In a thirteen-atom icosahedral cluster, there is one atom at the center of the nanoparticle, which we call core atom, surrounded by twelve atoms, which we call shell atoms. On the bare Au_{13} cluster, these twelve shell atoms are symmetrically equivalent, meaning that there are only two locations in the cluster where we can replace an atom: at the core or in the shell. For $Au_{12}X$ clusters with adsorbates, we now have three choices for where we can place the adsorbate relative to the X atom. Options for the relative position of the adsorbate to the X metal atom are: X in the center atom (C); X in the shell forming a direct bond with the adsorbate, which we call exterior-close (EC); and X in the shell with the adsorbate separated from X with by as much distance as possible, which we call exterior far (EF). These positions are illustrated in Figure 2.4. We recognize that there are many more possible configurations that molecules could adsorb on the clusters; however, since we are interested in screening possibly interesting compositions, and since we are using catalyst shapes that are likely unrealistic, we chose to only model the "limiting" cases.

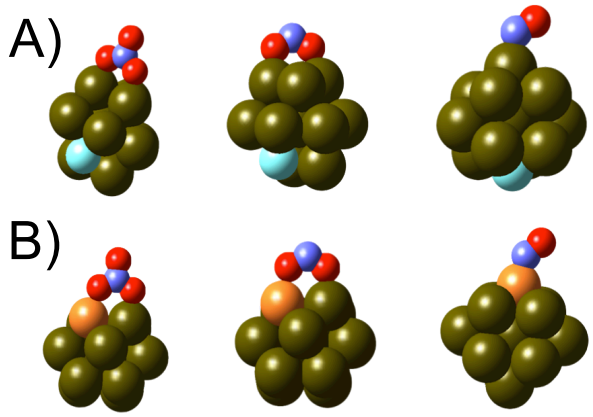

Figure 2.4 A)Exterior-Far and B) Exterior-Close type of adsorption for NO_3 (left), NO_2 (middle), and NO (right).

For each composition, we calculated reaction energies for NO_x (x = 3,2), H_2O, and NH_3 dissociation. Electronic structure calculations were performed with the VASP density functional theory (DFT) code[55-58], which is a periodic boundary condition, planewave basis set code. Another option we could have used was Gaussian 09[89], a code that uses the linear orbital approximation as opposed to the periodic planewave approach used in VASP. In the linear orbital approximation, the orbitals of atoms can be expressed as linear combinations of basis functions of atomic orbitals. The atomic orbitals used resemble hydrogen-like orbitals, since they can be expressed analytically. [90] The periodic planewave approach used in VASP describes the electronic structure of bulk and surface metals more accurately, but the linear orbital approximation as used in Gaussian09, works better for small molecules. Nanoparticles, which are small clusters of metal atoms, are neither surfaces nor molecules, so both codes could be used to model them. Choosing between both codes was not straightforward. We chose to work with VASP because with the orbital approach can be quite expensive when applied to metals, and in fact,

preliminary calculations used to test our methods that we performed with Gaussian09 were slow to converge. However, since VASP is used more for periodic structures such as bulk metals or surfaces, it is not necessarily the best code for simulating nanoparticles, which are non-periodic. Thus, we had to incorporate a number of features into our VASP calculations to minimize the effects of periodicity. (These are described below.) Additionally, VASP does not have a methodology for including solvation effects, but Gaussian 09 does. In hindsight, both codes have their pros and their cons, and if we could go back to the beginning and make a more educated choice about which code to use, we would choose VASP to optimize the metal atoms (the clean 13 atom nanoparticles) and then use Gaussian 09 to optimize the geometries of the adsorbates, while leaving the metal atoms fixed. More time should have been invested in choosing the right functional and basis set to optimize the accuracy and convergence in Gaussian 09.

Metal clusters were simulated in boxes with dimensions 20.0Å × 20.2Å × 20.4Å, large enough so that Coulombic interactions between neighboring periodic images were negligible (see appendix H) and slightly non-cubic in order to break the initial symmetries of the electronic structures, as this approach is more computationally efficient. We also found that using non-cubic boxes eliminated unphysical magnetic interactions between neighboring images; see Appendix I for a discussion.

Electron exchange and correlation were calculated using the Perdew-Burke-Ernzerhof (PBE) form of the generalized gradient approximation (GGA).[62] The ionic cores were modeled using the projector augmented wave (PAW)[91,92] pseudopotential method with an energy cut-off of 400 eV. Spin polarization was included because of the

magnetic natures of some of the metals. Electronic structures were considered to be converged when the energy difference between subsequent iterations fell below 10^{-5} eV. The k-point sampling, which is used to describe the frequency of the planewave through a crystal lattice, was done at the Γ point only, which is considered the center of the sampling space. Γ point calculations are typical for non-periodic systems. Geometries were considered to be converged when the forces on all adsorbate atoms fell below 0.03 eV/Å.

We used neutral NO_3 and NO_2 models for nitrate and nitrite. We did this because it is not straightforward to model charged systems using periodic codes, since the infinitely repeating cells would result in an infinite charge (something that we could have avoided had we used a non-periodic code like Gaussian 09). However, VASP has a method for charging the molecules in the system, while keeping the cell neutral by applying a countercharge to the vacuum space. We found, by performing Bader partial charge analysis, that the extra electron was delocalized in the nanoparticle itself instead of the adsorbate. The partial charge of the adsorbate remained relatively constant (the charge decreased by ~0.1 whether we used the neutral NO_x or the charged NO_x^- adsorbate; see Appendix J). Because of this the reactions that we studied were

$NO_3^* \rightarrow NO_2^* + O^*$ Equation 13

$NO_2^* \rightarrow NO^* + O^*$ Equation 14

$H_2O^* \rightarrow H^* + OH^*$ Equation 15

$NH_3^* \rightarrow NH_2^* + H^*$ Equation 16

where * denotes a catalyst site and *'ed species are bound to the catalyst. Favorable compositions should show exothermic behavior for both NO_x reactions and endothermic energies for Equations 14 and 15.

For NO_x we tested all three relative positions (C, EC, and EF) and used the one that yielded the lowest reaction energies using:

$$\Delta E_{rxn} = E_{products} - E_{reactants} \qquad \text{Equation 17}$$

where $E_{products}$ is the sum of the electronic energies of the products and $E_{reactants}$ is the sum of the electronic energy of the reactants. As an example, we can see in table 2.1 the reaction energies for NO_3 and NO_2 reduction for each of the three cases studied (C, EC, and EF) on $Au_{12}Cu$. When we add both reaction energies for the C, EC and EF cases we obtain 0.34 eV, 1.07 eV and 0.10 eV respectively. EF was chosen as the most favorable one because it gives the lowest added reaction energies.

Table 2.1 $Au_{12}Cu$ reaction energies in vacuum for C, EC and EF cases.

	Reaction Energy (eV)		
	NO_3*➔ NO_2* + O*	**NO_2*➔ NO* + O***	**sum**
C	-0.4	0.74	0.34
EC	-0.03	1.10	1.07
EF	**-0.18**	**0.28**	**0.10**

For H_2O and NH_3 we used the relative positions (C, EC, EF) that minimized the adsorption energy of the adsorbate of interest (either H_2O or NH_3).

The water surroundings need to be taken into account in the simulations, and modeling the water environment is not straightforward. In this work, solvation in water was included by using an implicit solvation model based on the iSMS model described by Faheem and Heyden.[93] Solvation energies were computed in Gaussian 09 using the converged geometries from VASP, both in the presence and absence of an implicit water solvent, and taking the difference

$$\Delta E_{solvation} = E_{solvated} - E_{vacuum} \qquad \text{Equation 18}$$

We can then estimate the reaction energy in aqueous phase by doing

$$\Delta E_{rxn}^{solv} = \Delta E_{rxn}^{vac} + \Delta E_{solvation\ 2} - \Delta E_{solvation1} \qquad \text{Equation 19}$$

where ΔE_{rxn}^{solv} is the reaction energy in a solvated environment, ΔE_{rxn}^{vac} is the reaction energy in a vacuum environment, $\Delta E_{solvation2}$ is the solvation energy of the products and $\Delta E_{solvation1}$ is the solvation energy of the reactants. Figure 2.5 shows a representation for the NO_3 reaction. We acknowledge the fact that problems may arise from the formed structure predicted by VASP not exactly matching that which would be found using Gaussian 09, but we assume a cancellation of errors takes place by adding and subtracting solvation energies.

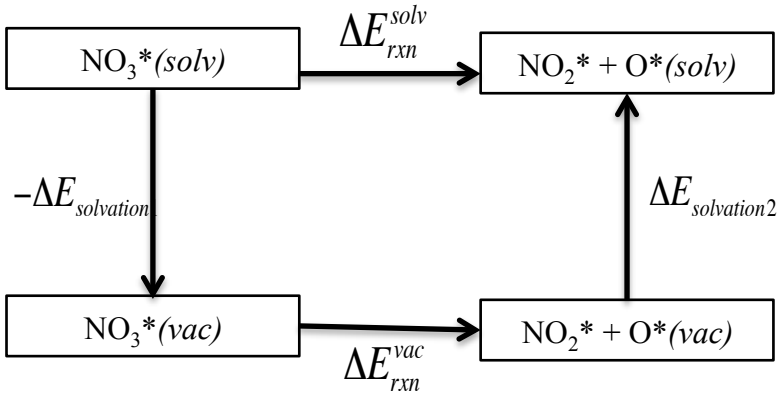

Figure 2.5 Diagram of solvation energy for NO_3 reaction. Reaction energies in vacuum ($\boldsymbol{\Delta E_{rxn}^{vac}}$) were obtained using VASP and solvation energies ($\Delta\, \boldsymbol{E_{solvation1}}$ and $\boldsymbol{\Delta E_{solvation2}}$) were obtained using Gaussian09.

The polarizable continuum model (PCM) [68] as implemented in Gaussian09 was used to model the water background. In all our Gaussian 09 calculations, we used the PBE exchange and correlation functional along with the 6-311+G(d,p) [94] basis set for light atoms and the LanL2DZ[95] effective core potential method for metals. The precision of the electronic structure calculations was set to 2 x 10^{-7}eV. Gaussian 09 calculations were performed at the single point only.

CHAPTER THREE

RESULTS AND ANALYSIS

2.3 Adsorption Energies

The adsorption energies and preferred sites for NO_3, NO_2, NO, NH_3, NH_2, OH and H on the Au_{13} catalyst models are collected in Table 3.1. We find that NO_3 ,NO_2, OH, and H adsorb preferably to a twofold site, while NO and H_2O preferably adsorb to an onefold site. Adsorption of NH_3 and NH_2 are endothermic for all three sites. The optimized structures are presented in Figure 3.1.

Table 0.1 Adsorption energies (eV) for different species on the Au_{13} nanoparticle in vacuum. Bold represents the most favorable adsorption site for each molecule. The dashes represent values that did not converge.

	Onefold	**Twofold**	**Threefold**
NO_3	-	**-1.62**	-1.35
NO_2	-1.07	**-1.42**	-0.88
NO	**-1.16**	-1.13	-0.47
NH_3	**1.46**	2.51	2.57
NH_2	**0.61**	2.65	-
H_2O	**-0.29**	-0.03	0.00
OH	-2.37	**-2.50**	-2.37
H	-0.26	**-0.34**	2.31

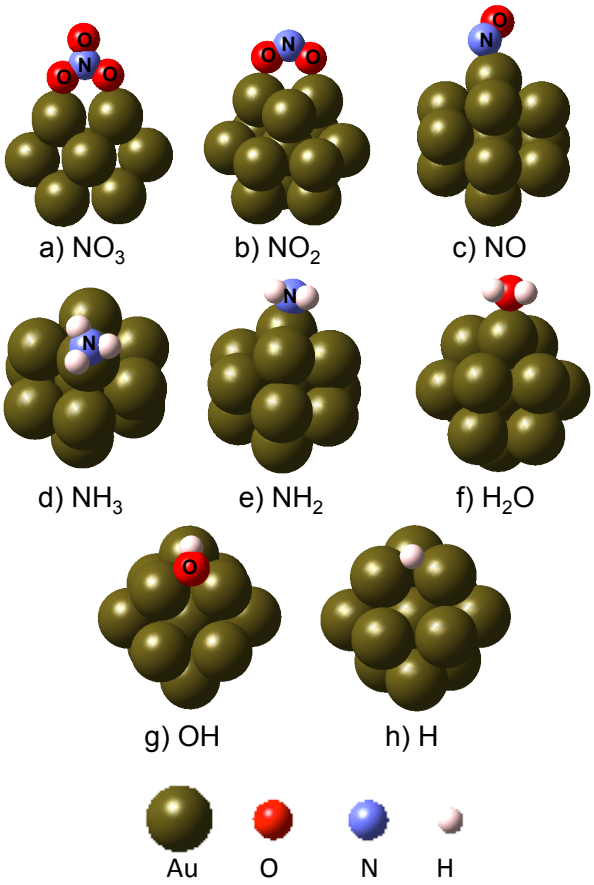

Figure 0.1 Au nanoparticle with different adsorbates on their most favorable adsorption sites

2.4 Dissociation thermodynamics of NO_3 and NO_2 on $Au_{12}X$ nanoparticles

In this section, NO_3 and NO_2 dissociation energies on the different $Au_{12}X$ catalyst compositions studied are discussed (see Table 3.2). For X = Cu, Fe and In, the most favorable position of the X atom was the EF case, meaning the X atom was the furthest from the adsorbates. For X= Pd the most favorable position of the X atom was the EC case, meaning when the X atom was the closest to the adsorbates.

For all our studied catalysts, NO_3 dissociation was exothermic, with reaction energies ranging from -0.21 eV to -0.9 eV. NO_2 dissociation energies showed endothermic behavior, varying from 0.02 eV to 1.77 eV. This tells us that it is critical to design a catalyst composition to break an O—NO bond. From all the compositions tested, $Au_{12}Pd$ and $Au_{12}Fe$ gave the biggest downshift in energy from pure Au_{13}, making Pd and Fe the most promising metals for alloying with Au for NO_3 and NO_2 dissociation, amongst the compositions tested.

Table 0.2 Reaction energies for NO_3 and NO_2 reduction on different $Au_{12}X$ catalysts in vacuum. The most favorable position of the X atom, determined as that where the average reaction energy is the lowest, is in bold.

		Reaction Energy (eV)	
		NO_3* → NO_2* + O*	**NO_2* → NO* + O***
Au_{13}		**-0.09**	**0.79**
$Au_{12}Pd$	C	-0.21	0.83
	EC	**-0.21**	**0.15**
	EF	-0.07	0.71
$Au_{12}Fe$	C	0.01	1.03
	EC	-0.06	-0.07
	EF	**-0.14**	**0.02**
$Au_{12}Cu$	C	-0.40	0.74
	EC	-0.03	1.10
	EF	**-0.18**	**0.28**
$Au_{12}In$	C	-0.12	1.42
	EC	0.29	1.56
	EF	**-0.15**	**1.77**

2.5 Descriptors for NO_2 reduction

Figure 3.2 shows the dissociation energies of NO_3 and NO_2 for the most favorable case (EC, C, or EF) plotted versus the d band center of the bulk X metal (Au, Cu, Pd, In, Fe). While the dissociation of NO_3, remains essentially constant through all the catalysts and does not correlate to the d band center, NO_2 dissociation does linearly correlate to the d band center of the bulk metal, which leads us to believe that NO_2 dissociation could be an important descriptor that could be used when screening catalysts for NO_3 and NO_2 reduction.

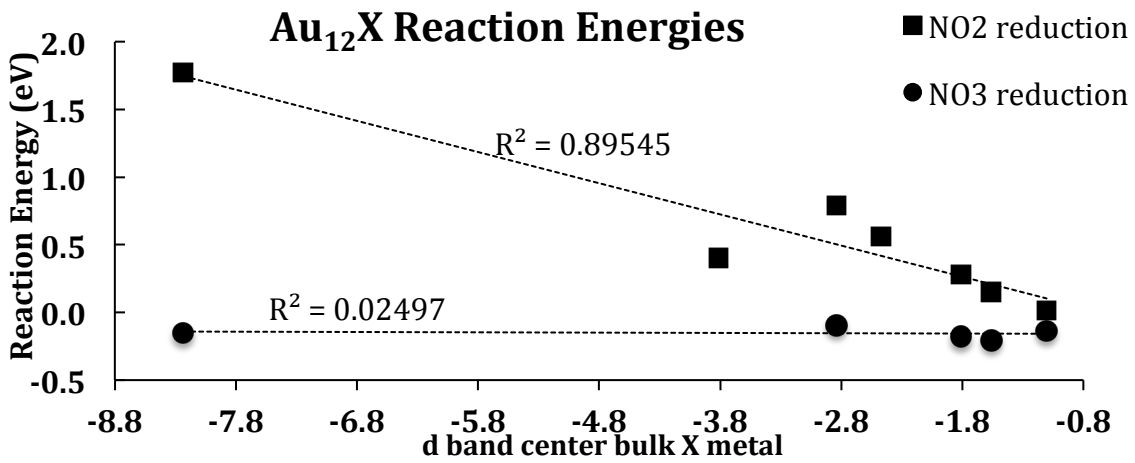

Figure 0.2 Reaction energies in water vs. d band center of X bulk metal in $Au_{12}X$ nanoparticles

Using the NO_2 dissociation energies presented in table 3.2 and different parameters calculated (see appendix L and appendix O), correlations and trends were found.

Fig. 3.3 shows when the alloying X atom is found at the center (C) or at the exterior-close position (EC) the dissociation energy of NO_2 in water is directly correlated to the adsorption energy of NO to the nanoparticle in vacuum. The stronger the adsorption (lower Eads) of NO, the lower is the dissociation energy for NO_2. At first glance, this suggest that we should identify catalysts with strong NO adsorption energies however, based on the Sabatier principle, the optimum adsorption energy should be an intermediate value that allows the NO to react into products. If we wanted to prove this, NO dissociation energies would be needed.

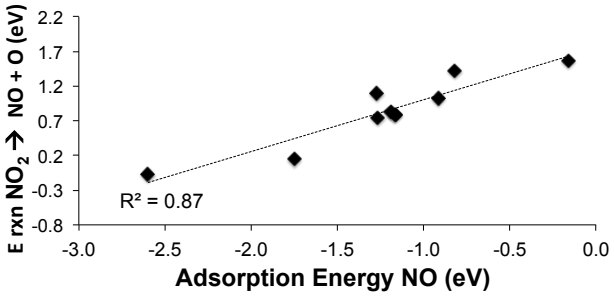

Figure 0.3 Linear correlation of NO2 dissociation energies in water (eV) vs. NO adsorption energy in vacuum (eV) for C and EC cases.

For the case when the alloying atom is in the exterior and the furthest from the adsorbates the NO_2 dissociation energy correlates to the charge of the X atom when NO is adsorbed (See figure 3.4). When the charge is higher, the reaction energy is more negative. This shows that the alloying metal plays a big role even when it's the furthest from the adsorbates by donating charge to allow back donation of electrons. We note here that that for X=In, it did not fit the trend. The charge of In was negative when NO adsorbed and the charge of the adsorbate NO was positive, indicating that the charge was

going from NO to the nanoparticle. Therefore, it was not included in the plot. We hypothesize that these trends, and thus the conclusions made using them, only apply to metals with d and s (not p) orbitals in the valency.

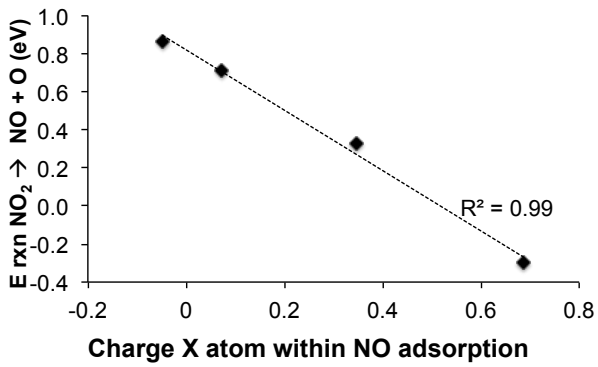

Figure 0.4 Linear correlation of NO_2 dissociation energies in water (eV) vs. charge of X atom when NO is adsorbed for EF case. Partial charge was calculated suing Bader algorithm for Henkelman charge analysis

2.6 Comparison of NO_3, NO_2 dissociation with NH_3, H_2O dissociation

To chemically convert nitrate into benign products, we need to select catalysts that selectively reduce nitrate instead of water and other dissolved contaminants. As discussed in Chapter 1, the number of potential contaminants in water is innumerable; therefore, we must focus on either the most important contaminants or the most popular ones for the sake of computational tractability. For these screening calculations, we have chosen to test catalytic selectivity toward nitrate over water and amines. We have chosen water because it can chemically convert transition metals into oxides, hydroxides, and other forms, which will almost assuredly promote different chemistry than the metals themselves, which may or may not even be active as catalysts. For example, a purely Fe

catalyst would hypothetically turn to rust and deactivate in a water environment. Thus, we seek a catalyst that is relatively inactive toward water. We have chosen amines because they are organic chemicals commonly dissolved in natural waters[96]. NH_3 is the simplest amine. We chose to use NH_3 in order to minimize the computational effort, since the number of possible decomposition products will be relatively small. For all of our catalysts tested, NH_3 and H_2O dissociation were endothermic, which is promising. For one, even in the absence of kinetic calculations, the reaction energies for endothermic reactions provide the *minimum* activation energies. Thus, for NH_3 dissociation, the minimum activation energy is ~ 0.8 eV on our catalyst models. The reaction energies for H_2O, while all endothermic, range from 0.2 to 0.7eV. Finally, we recognize that a catalyst's actual preference for dissociation depends not only on the reaction electronic energy, but also on other quantities, such as entropy and concentration. While we expect amines to be present at relatively small concentrations in water, the concentration of water itself will be large, and likely much larger than the concentration of nitrate. It is thus possible that our catalysts will dissociate H_2O to at least some extent. Further modeling, specifically performing kinetic calculations, is needed in order to identify catalysts that are inactive towards H_2O.

Table 0.3 Dissociation energies of NH_3 and H_2O on the different catalysts in water

	Dissociation Energies (eV)	
	$NH_3^* \rightarrow NH_2^* + H^*$	$H_2O^* \rightarrow H^* + OH^*$
Au_{13}	1.11	0.63
$Au_{12}Pd$	1.04	0.41
$Au_{12}Fe$	0.84	0.19
$Au_{12}Cu$	0.83	0.62
$Au_{12}In$	1.03	0.74

2.7 Dissociation thermodynamics of NO_3 and NO_2 on $Au_{11}XY$ nanoparticles

Since $Au_{12}Fe$ and $Au_{12}Pd$ gave us the most favorable dissociation energies, we proceeded to compute the same reactions on $Au_{11}XY$ catalysts, where X/Y = Fe, Pd (Figure 3.5). We found that replacing two atoms followed the same pattern as $Au_{12}X$ energies in that NO_3 dissociation energies remained exothermic and NO_2 dissociation energies seemed to be affected more. NO_3 dissociations energies ranged from -0.09 to -0.33 eV. NO_2 dissociation energies varied from 0.39 eV for $Au_{11}Pd_2$, to -0.81 eV for $Au_{12}FePd$ and -1.0 eV for $Au_{11}Fe_2$. With $Au_{11}FePd$ and $Au_{11}Fe_2$ we see the expected downshift in energy, but for $Au_{11}Pd_2$ we see there is a slight increase in dissociation energy from $Au_{12}Pd$ and it stays endothermic. We also computed the dissociation energies for $Au_{11}Pd_2$ with the two Pd atoms further apart from each other and similar reaction energetics where obtained.

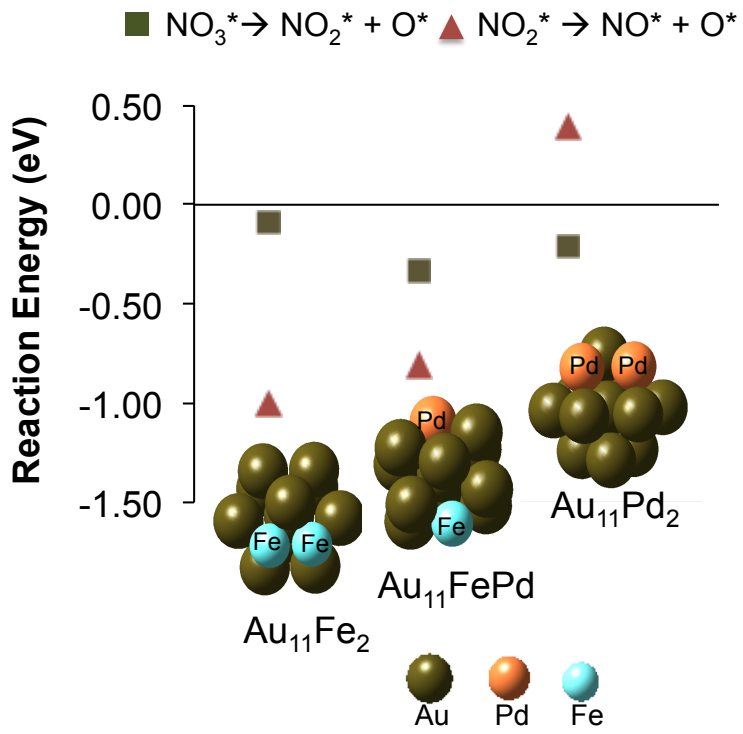

Figure 0.5 Dissociation of NO_3 and NO_2 on $Au_{11}XY$ nanoparticles in water.

CHAPTER FOUR

SUMMARY, DISCUSSION, CONCLUSIONS, AND RECOMMENDATIONS FOR FUTURE WORK

With DFT simulations, we screened for Au-based catalyst compositions that are thermodynamically favorable towards nitrate and nitrite reduction. We also initiated a study on the selectivity of the catalysts of nitrate and nitrite decomposition versus water and ammonia decomposition. We found that all of our $Au_{12}X$ catalyst tested showed exothermic behavior towards NO_3 dissociation, endothermic behavior towards H_2O and NH_3 dissociation, and a large range of energies for NO_2 dissociation. While NH_3 dissociation was always quite endothermic, H_2O dissociation energies varied more with some being as low as 0.2 eV. Thus, H_2O dissociation could be favorable under certain conditions. We found that the energies of NO_2 dissociation could be correlated to the d band center of the bulk X metal, which led us to believe that NO_2 dissociation could be used as a descriptor for nitrate reduction, but we need to be cautious because the most favorable catalysts for NO_2 dissociation were the ones that also favored H_2O dissociation. Our results to this point indicate that Au-based catalysts should be capable of dissociating NO_3 and incapable of dissociating NH_3 but that their activities toward NO_2 and H_2O dissociations are variable. Future work should involve honing in on a catalyst that exhibits a modestly exothermic reaction energy for NO_2 dissociation and a largely endothermic reaction energy or kinetically impossible activation energy for H_2O dissociation. Our results suggest that this catalyst will display an appropriately balanced adsorption energy for NO_2, which based on the Sabatier principle should be strong

enough to promote NO_2 dissociation, but not so strong as to inhibit NO dissociation. It should also possess two types of metals: 1) a stable, non-reactive material such as gold, to avoid water dissociation and allow us to carefully tune for selectivity, and 2) one or more materials with strong electron donation properties, as these materials promote NO_2 reduction.

A screening strategy that could be implemented to test the reaction energies is to compute the difference in reaction energies of NO_2 dissociation and H_2O dissociation as a descriptor.

$$\Delta E_{\text{descriptor}} = \Delta E_{rx\ \text{NO2}} - \Delta E_{rx\ \text{H2O}} \qquad \text{Equation 20}$$

Since $\Delta E_{rx\ \text{NO2}}$ needs to be low and $\Delta E_{rx\ \text{H2O}}$ needs to be high, $\Delta E_{\text{descriptor}}$ should be as low as possible for it to favor NO_2 dissociation over H_2O dissociation. The $\Delta E_{\text{descriptor}}$ computed for our different $Au_{12}X$ catalysts is presented in table 4.1

Table 4.1 $\Delta E_{\text{descriptor}}$ (eV) for $Au_{12}X$ catalysts in water as screening method

Catalyst	$\Delta E_{\text{descriptor}}$ **(eV)**
$Au_{12}Cu$	-0.34
$Au_{12}Pd$	-0.26
$Au_{12}Fe$	-0.17
Au_{13}	0.16
$Au_{12}In$	1.04

If only dissociation energies of NO_2 are studied as a screening factor, out of the $Au_{12}X$ catalysts tested, one would say that the most favorable compositions are $Au_{12}Fe$ and $Au_{12}Pd$. But if the screening technique is implemented and the different $\Delta E_{\text{descriptor}}$

values are studied, which include NO_2 and H_2O dissociation, the most favorable catalysts would be $Au_{12}Cu$ (See table 4.1). In reality, a more appropriate descriptor would be something like a free energy, which would take the chemical potentials of NO_2 and H_2O into account. Given that the chemical potential of H_2O is likely significantly larger than that of NO_2 in the waters under consideration, a large separation in reaction energies is likely quite important.

Our results for $Au_{11}XY$ catalysts were done with X/Y = Fe, Pd because they seemed like the most favorable metals, but now it can be seen that X/Y = Cu should have been included as well. The results showed that $Au_{11}Fe_2$ and $Au_{11}FePd$ were very favorable for NO_3 and NO_2 dissociation, with highly exothermic reactions, but to be able to complete the analysis, H_2O dissociation energies should be computed as well to be able to calculate $\Delta E_{\text{descriptor}}$.

After studying the thermodynamic behavior of gold-based nanoparticles for nitrate reduction, the next immediate step should be to study the kinetics of NO_x dissociation and H_2O dissociation. All this kinetic analysis should be done in the most favorable catalysts and/or other materials with similar properties. The characteristics that this catalyst should have can be deduced from the material properties we found in our analysis. For example, if we decide to keep using gold, we know we would probably have to "dope" the gold with another metal, probably a metal from groups 8, 9, or 10 from the periodic table, since these metals will have similar electronic properties to Fe, Cu and Pd, our most favorable alloying metals. This is similar to what has been found on the literature where palladium bimetallic catalysts (Pd–Cu, Pd–Sn, Pd–In and Pd–Zn)

showed the most favorable results for nitrate and nitrite reduction[32,33]. Also, the doping metal should be able to be a strong electron donor, as our Bader charge analysis showed that strong electronic donation favored NO_2 dissociation. The catalyst should bind to the intermediate compounds (NO_2, NO) following the Sabatier principle with "optimum strength of bonding". To make sure of this, NO dissociation should also be computed. This could be done in a similar manner as NO_3 and NO_2 dissociation was done in this work:

$$NO^* \rightarrow N^* + O^* \qquad \text{Equation 21}$$

Alternatively, we could identify catalyst supports that induce the same properties in Au-based catalysts as the dopant metals do in the unsupported catalysts. Ligated nanoparticles could also provide the support and still present the desired catalytic properties.

Another direction could be to move towards another pollutant. Like it was mentioned in chapter 1, there is a need for remediation of rising concentrations of emerging contaminants such as pharmaceutical and personal care products (PPCP). Their recalcitrant chemical structures make it difficult to decompose and neutralize them using the traditional methods for water and wastewater remediation. δ-valerolactone could be used as model because of it's small but recalcitrant structure, making it a good candidate for simulating the properties of PPCP, while still being computationally efficient.

I would suggest computing a key reaction on the catalysts tested, which would involved breaking a C=C bond of the ring and it's hydrogenation to form pentane-1,5-diol.

$$C_5H_8O_2^* + 4H^* \rightarrow C_5H_{12}O_2 \qquad \text{Equation 22}$$

And with the same method described in this thesis, compare to the dissociation of water and ammonia or other competitor compounds of interest.

APPENDICES

Appendix A

Au_{13} nanoparticle : adsorbate binding and relative energies

Adsorption energies were calculated in order to find the most favorable adsorption site for NO, NO_2 and NO_3 on the 13 atom gold nanoparticle using Equation 4. NO-O and NO_2-O adsorption energies were also calculated at two cases: oxygen being the furthest from the the adsorbate and being the closest.

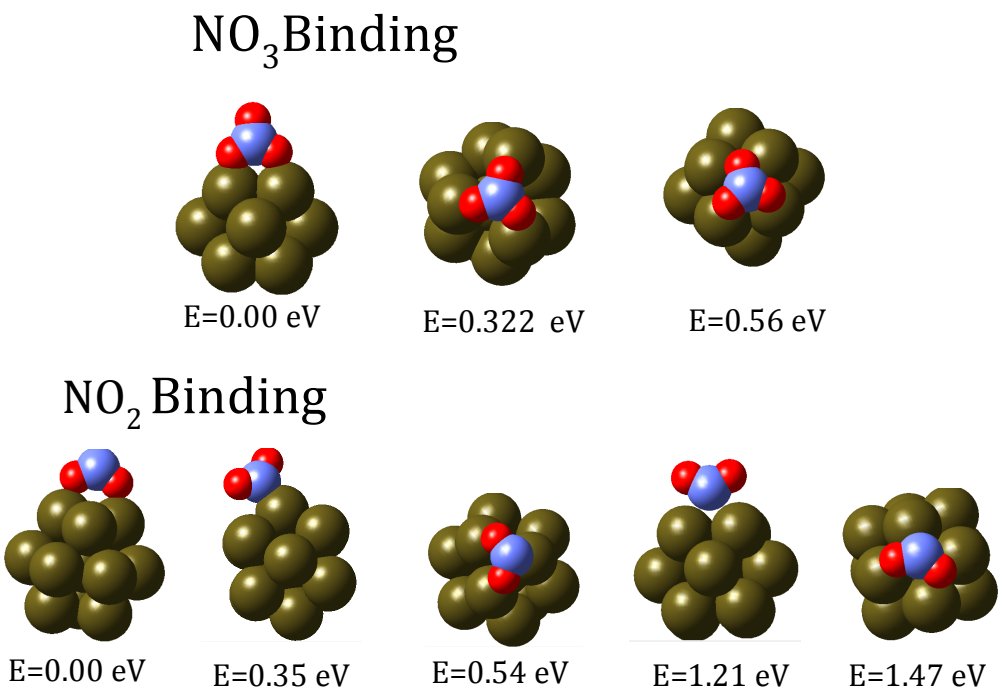

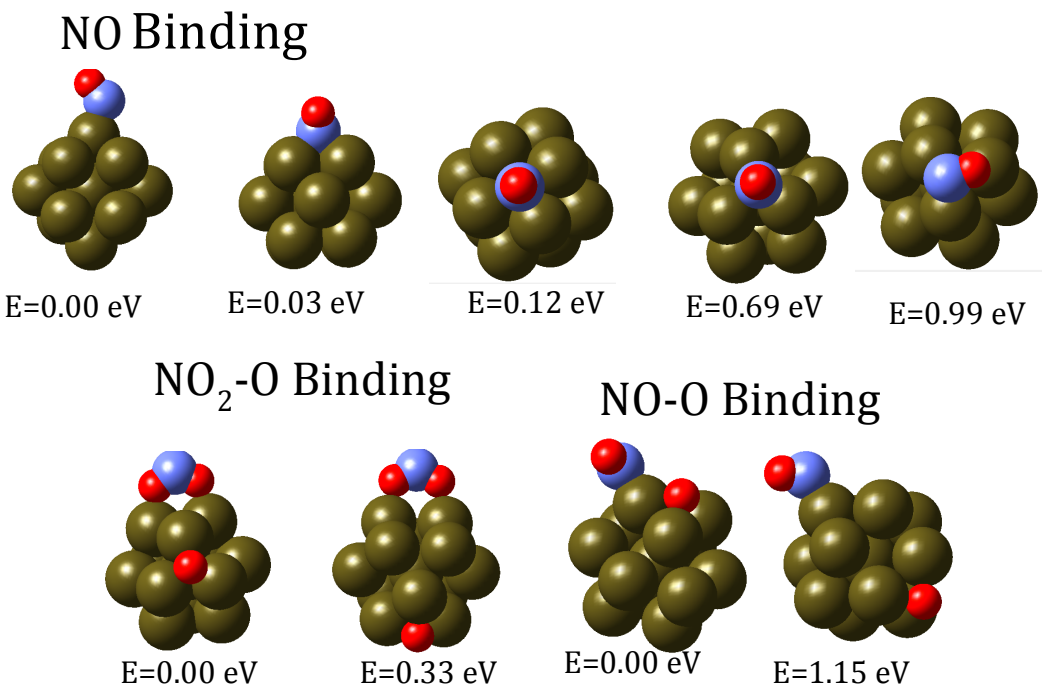

Are the NO2+O and NO+O in the right order? (so the lateral interactions are opposite of what they are on surfaces?)

Appendix B

Cost and toxicity of metals

In order to alternate the catalytic properties of the Au_{13} cluster, one atom was replaced with another metal. The metals used had to be representative of a particular region within the periodic table. The elements in the periodic table were split into groups and to decide which metal to use we got their cost and their toxicity. Based on those two factors we picked one from each group to create $Au_{12}X$ nanoparticles.

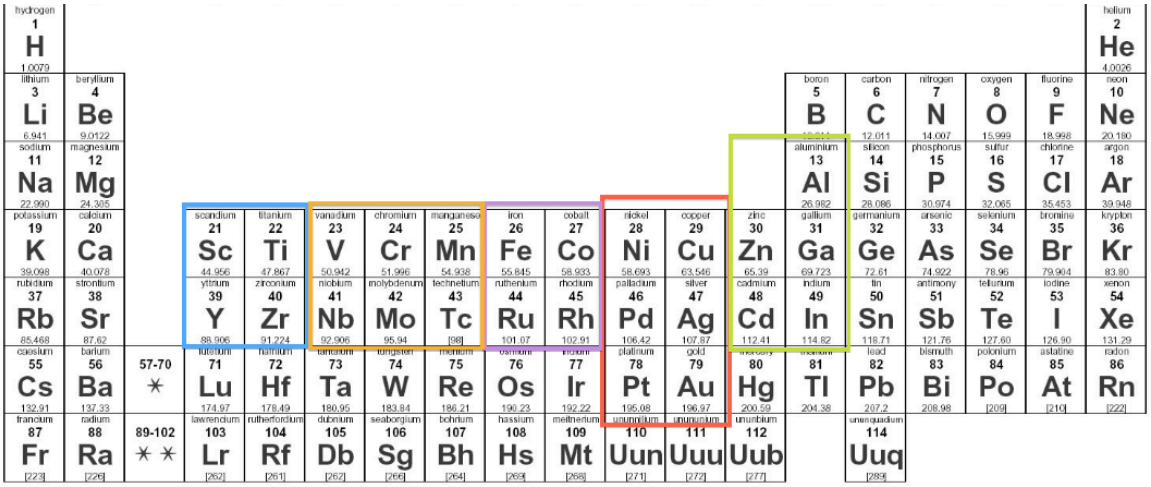

Group1	Price ($/g)	toxicity
Sc	18	non toxic
Ti	6.6	non toxic
Y	0.17	mildly toxic
Zr	1.57	low toxicity

Group 2	Price ($/g)	toxicity
V	0.014	mildly toxic
Cr	0.32	highly toxic
Mn	0.003	low toxicity
Nb	0.18	non toxic
Mo	0.033	low toxicity
Tc	60	low toxicity

Group3	Price ($/g)	toxicity
Fe	0.072	mildly toxic
Co	0.031	highly toxic
Ru	3.53	higly toxic
Rh	51.84	non toxic

Group4	Price ($/g)	toxicity
Ni	0.018	mildly toxic
Cu	0.007	mildly toxic
Pd	21.22	mildly toxic
Ag	0.93	low toxicity
Pt	45.95	low toxicity

Group5	Price ($/g)	toxicity
Al	0.0019	non toxic
Zn	0.0018	low toxicity
Ga	2.2	non toxic
Cd	0.003	Higly toxic
In	0.7	non toxic

Price and toxicity estimates where obtained from the following sources:

Group1:

http://www.mineralprices.com/default.aspx#Rare
http://www.chemicool.com/elements/titanium.html
http://www.mineralprices.com/default.aspx#Rare
http://www.chemicool.com/elements/zirconium.html
http://en.wikipedia.org/wiki/Scandium#Health_and_safety
http://en.wikipedia.org/wiki/Titanium#Precautions
http://en.wikipedia.org/wiki/Yttrium#Precautions
http://en.wikipedia.org/wiki/Zirconium#Safety

Group2:

http://www.mineralprices.com/default.aspx#Rare
http://www.chemicool.com/elements/chromium.html
http://www.mineralprices.com/default.aspx#Rare
http://www.chemicool.com/elements/niobium.html
http://www.mineralprices.com/default.aspx#Rare
http://www.hobart.k12.in.us/ksms/PeriodicTable/technetium.htm
http://en.wikipedia.org/wiki/Vanadium#Safety
http://en.wikipedia.org/wiki/Chromium#Precautions
http://en.wikipedia.org/wiki/Manganese#Precautions
http://en.wikipedia.org/wiki/Niobium#Precautions
http://en.wikipedia.org/wiki/Molybdenum#Precautions
http://en.wikipedia.org/wiki/Technetium#Precautions

Group3:

http://www.chemicool.com/elements/iron.html
http://www.mineralprices.com/default.aspx#Rare
http://www.mineralprices.com/default.aspx#Rare
http://www.mineralprices.com/default.aspx#Rare
http://en.wikipedia.org/wiki/Iron#Precautions
http://corrosion-doctors.org/Elements-Toxic/Cobalt.htm
http://www.lenntech.com/periodic/elements/ru.htm
http://en.wikipedia.org/wiki/Rhodium#Precautions

Group4:

http://www.mineralprices.com/default.aspx#Rare
http://www.mineralprices.com/default.aspx#Rare
http://www.mineralprices.com/default.aspx#Rare

http://www.mineralprices.com/default.aspx#Rare
http://www.mineralprices.com/default.aspx#Rare
http://www.mineralprices.com/default.aspx#Rare
http://en.wikipedia.org/wiki/Nickel#Toxicity
http://en.wikipedia.org/wiki/Copper#Precautions
http://en.wikipedia.org/wiki/Palladium#Precautions
http://en.wikipedia.org/wiki/Silver#Human_exposure_and_consumption
http://en.wikipedia.org/wiki/Platinum#Health_issues

Group5:
http://www.mineralprices.com/default.aspx#Rare
http://www.mineralprices.com/default.aspx#Rare
http://www.chemicool.com/elements/gallium.html
http://www.mineralprices.com/default.aspx#Rare
http://www.mineralprices.com/default.aspx#Rare
http://en.wikipedia.org/wiki/Aluminium#Health_concerns
http://en.wikipedia.org/wiki/Zinc_toxicity
http://en.wikipedia.org/wiki/Gallium#Precautions
http://corrosion-doctors.org/Elements-Toxic/Cadmium.htm
http://en.wikipedia.org/wiki/Indium#Precautions_and_health_issues

Appendix C

Reaction energies in vacuum $Au_{12}X$

Reaction energies for the reduction of NO_3 and NO_2 on the different catalysts were obtained using

$$\Delta E_{rxn} = E_{products} - E_{reactants}$$

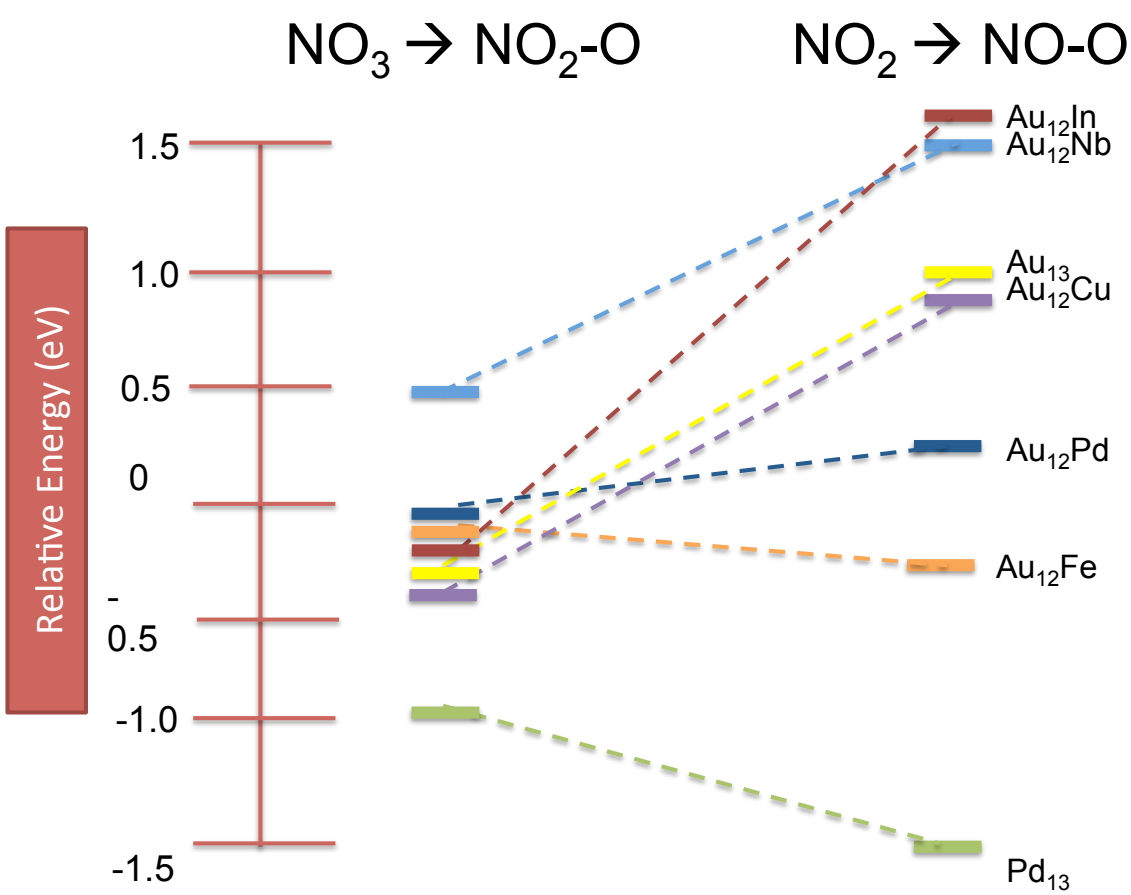

Appendix D

Bulk FCC Au

To be able to obtain the lattice constant for bulk Au, we converged the kpoints and the lattice of the cell.

K points convergence

Kpoints	Irreducible Kpoints	Energy
3	14	-3.5775
4	36	-2.9794
5	63	-3.3023
6	112	-3.1174
7	172	-3.2466
8	260	-3.1529
9	365	-3.2185
10	504	-3.1714
11	666	-3.2027
12	868	-3.1845
13	1099	-3.1961
14	1376	-3.1919
15	1688	-3.1928

ODD			
Mesh	**Irreducible**	**Energy (eV)**	**time (s/elec)**
3	14	-3.577486	0.439461538
5	63	-3.302334	1.180538462
7	172	-3.246559	2.801846154
9	365	-3.218506	6.423923077
11	666	-3.202687	11.21869231
13	1099	-3.196148	26.468
15	1688	-3.192779	67.00815385

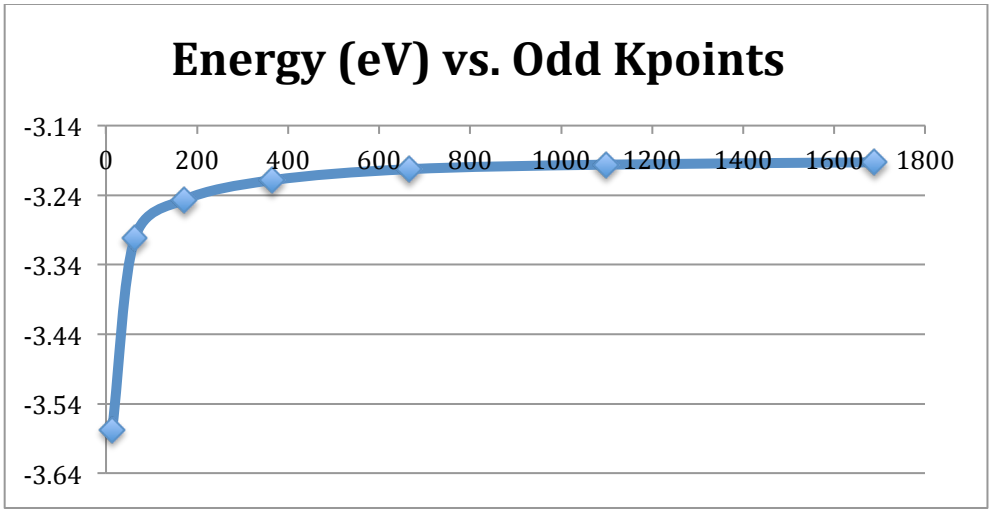

EVEN			
Mesh	**Irreducible**	**Energy (eV)**	**time (s/elec)**
4	36	-2.9794	0.707428571
6	112	-3.117423	2.954461538
8	260	-3.152864	3.683153846
10	504	-3.171406	14.00876923
12	868	-3.184482	12.95884615
14	1376	-3.191922	29.831

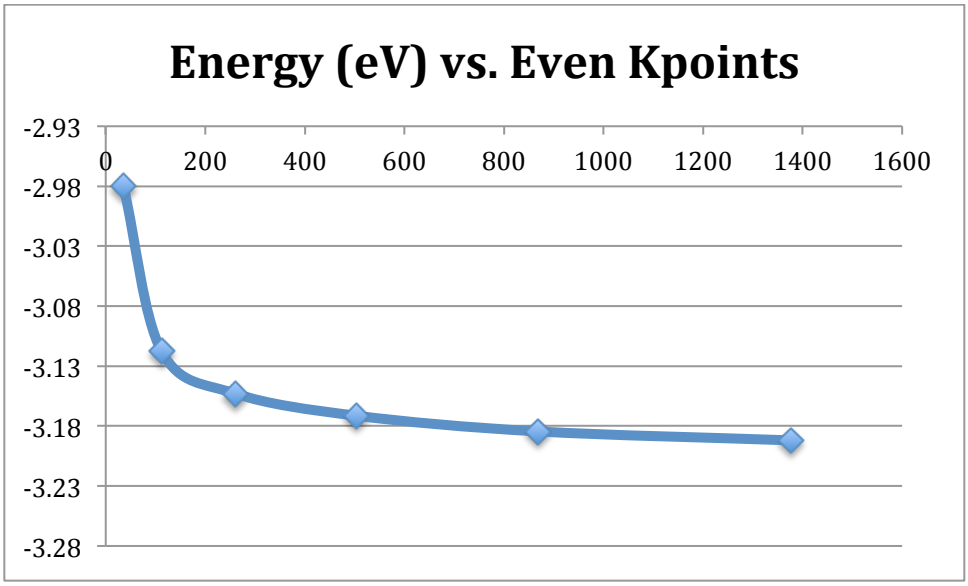

Lattice convergence

Experimental lattice constant: 4.08 Å[86]

lattice (Å)	Energy (eV)
3.90	-11.41
3.95	-11.99
4.00	-12.40
4.05	-12.68
4.10	-12.76
4.15	-12.89
4.20	-12.86
4.25	-12.76

lattice (Å)	Energy (eV)	lattice (Bohr)	Energy (Ry)
4.11	-12.8503	7.7668	-0.9445
4.12	-12.8650	7.7857	-0.9456
4.13	-12.8760	7.8046	-0.9464
4.14	-12.8837	7.8235	-0.9469
4.15	-12.8879	7.8424	-0.9472
4.16	-12.8888	7.8613	-0.9473
4.17	-12.8864	7.8802	-0.9471
4.18	-12.8810	7.8991	-0.9467
4.19	-12.8725	7.9180	-0.9461

Converged	
lattice (Å)	Energy (eV)
4.15747381	-12.888868

Appendix E

Bulk BCC Fe

To be able to obtain the lattice constant for bulk Fe, we converged the kpoints and the lattice of the cell.

Kpoints

Kpoints	Irreducible Kpoints	Energy (eV)
3	14	-8.2757
4	36	-8.2240
5	63	-8.1787
6	112	-8.2739
7	172	-8.2479
8	260	-8.2263
9	365	-8.2335
10	504	-8.2365
11	666	-8.2357
12	868	-8.2366
13	1099	-8.2297
14	1376	-8.2372
15	1688	-8.2354

ODD			
Mesh	**Irreducible**	**Energy (eV)**	**time (s/elec)**
3	14	-8.2757	1.4123
5	63	-8.1787	3.0013
7	172	-8.2479	6.5189
9	365	-8.2335	14.2551
11	666	-8.2357	20.5778
13	1099	-8.2297	26.9516
15	1688	-8.2354	52.6431

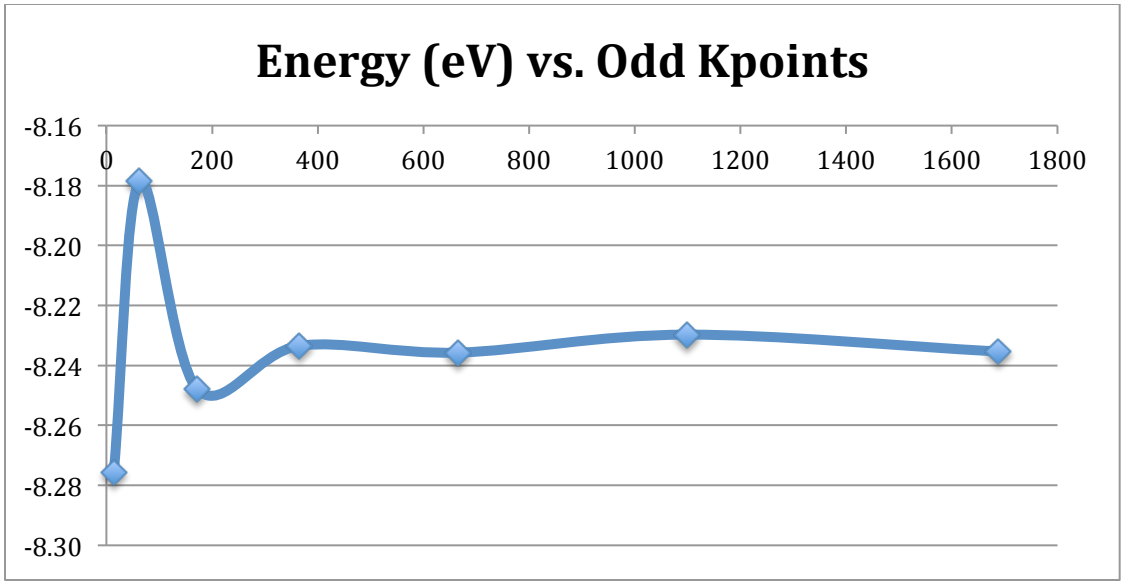

EVEN			
Mesh	**Irreducible**	**Energy (eV)**	**time (s/elec)**
4	36	-8.2240	1.9641
6	112	-8.2739	4.5495
8	260	-8.2263	8.5191
10	504	-8.2365	18.9042
12	868	-8.2366	27.5385
14	1376	-8.2372	30.6738

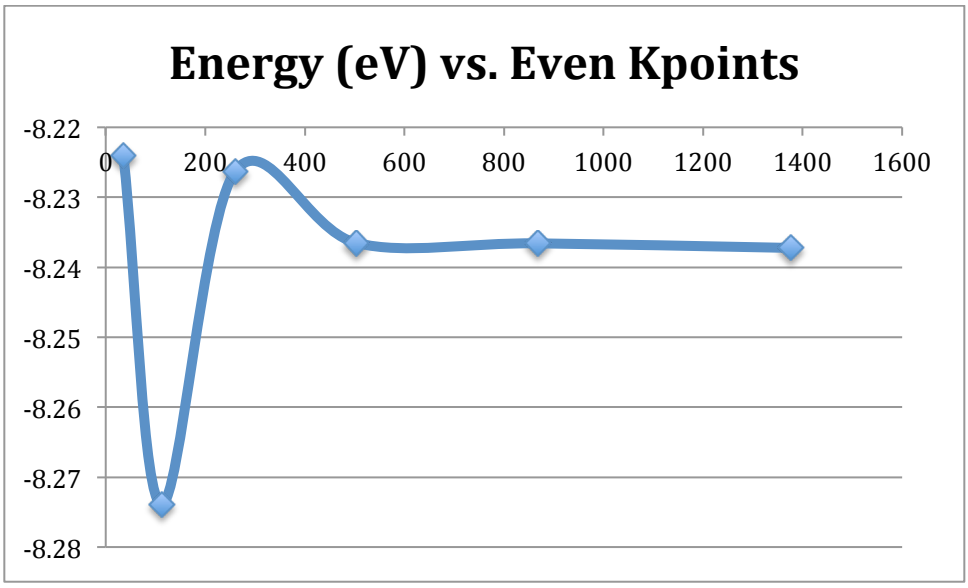

Lattice convergence

Experimental lattice constant: 2.87 Å[86]

Lattice (Å)	Energy (eV)
2.70	-16.1799
2.75	-16.3810
2.80	-16.4748
2.85	-16.4792
2.90	-16.4206
2.95	-16.3195
3.00	-16.1813
3.05	-16.0099

Lattice (Å)	Energy (eV)	lattice (Bohr)	Energy (Ry)
2.81	-16.4823	5.3101	-1.2114
2.82	-16.4866	5.3290	-1.2117
2.83	-16.4870	5.3479	-1.2118
2.84	-16.4844	5.3668	-1.2116
2.85	-16.4792	5.3857	-1.2112
2.86	-16.4726	5.4046	-1.2107
2.87	-16.4635	5.4235	-1.2100
2.88	-16.4517	5.4424	-1.2092
2.89	-16.4373	5.4613	-1.2081

Converged

lattice (Å)	Energy (eV)
2.82651692	-16.487238

Appendix F

Bulk FCC Pd

To be able to obtain the lattice constant for bulk Pd, we converged the kpoints and the lattice of the cell.

Kpoints

Kpoints	Irreducible Kpoints	Energy (eV)
3	14	-4.3389
4	36	-5.3509
5	63	-5.0401
6	112	-5.2131
7	172	-5.2070
8	260	-5.1816
9	365	-5.2102
10	504	-5.2185
11	666	-5.1895
12	868	-5.2053
13	1099	-5.2070
14	1376	-5.1925
15	1688	-5.2103

ODD			
Mesh	**Irreducible**	**Energy (eV)**	**time (s/elec)**
3	14	-4.3389	1.5676
5	63	-5.0401	3.2593
7	172	-5.2070	4.2625
9	365	-5.2102	7.7961
11	666	-5.1895	16.0064
13	1099	-5.2070	22.7563
15	1688	-5.2103	34.3526

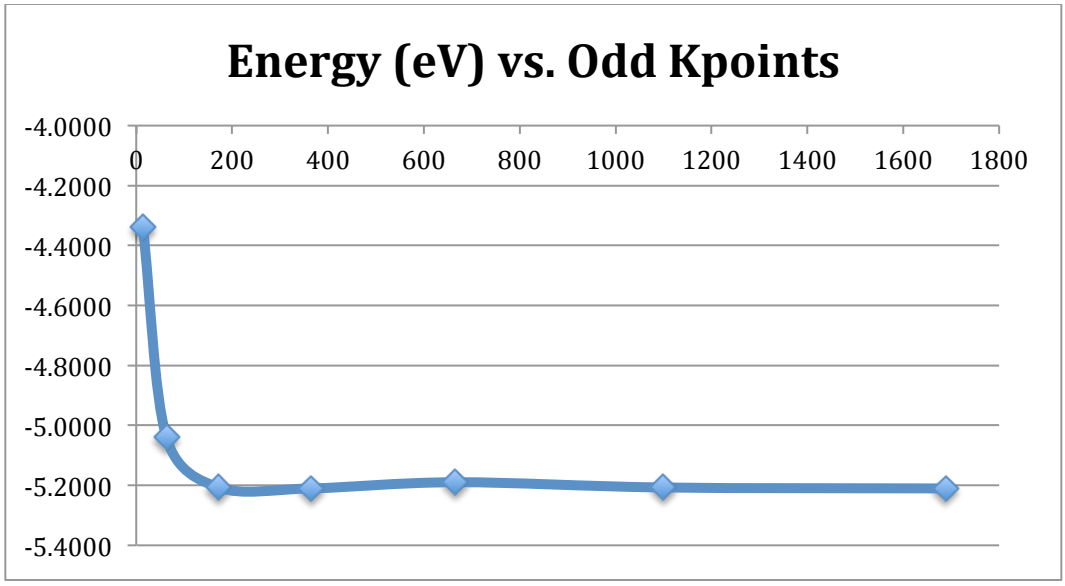

EVEN			
Mesh	**Irreducible**	**Energy (eV)**	**time (s/elec)**
4	36	-5.3509	3.1976
6	112	-5.2131	2.7789
8	260	-5.1816	5.6437
10	504	-5.2185	10.9396
12	868	-5.2053	20.5200
14	1376	-5.1925	46.9257

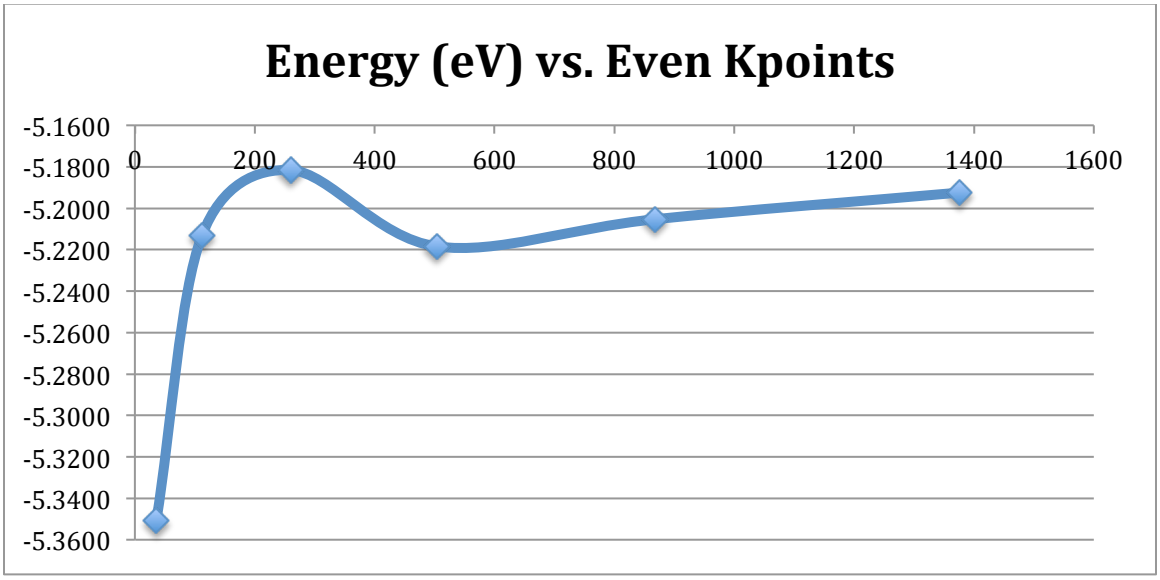

Lattice convergence

Experimental lattice constant: 3.89 Å[86]

lattice (Å)	Energy (eV)
3.70	-19.4278
3.75	-20.0143
3.80	-20.4269
3.85	-20.6913
3.90	-20.8292
3.95	-20.8585
4.00	-20.7991
4.05	-20.6625

lattice (Å)	Energy (eV)	lattice (Bohr)	Energy (Ry)
3.91	-20.8433	7.3888	-1.5320
3.92	-20.8533	7.4077	-1.5327
3.93	-20.8591	7.4266	-1.5331
3.94	-20.8612	7.4455	-1.5333
3.95	-20.8585	7.4644	-1.5331
3.96	-20.8543	7.4833	-1.5328
3.97	-20.8452	7.5022	-1.5321
3.98	-20.8331	7.5211	-1.5312
3.99	-20.8171	7.5400	-1.5300

Converged

lattice (Å)	Energy (eV)
3.93980089	-20.846932

Lattice constants for bulk In and Cu were calculated by members of the Getman Group.

In by Andrew Mccartney and Cu by Heather Rodgers.

Appendix G

Energy of molecules on Vasp

To be able to calculate adsorption energies, the gas phase energies of different molecules are needed.

Molecule	Energy (eV)
CH_3OH	-30.228474
CH_4	-24.031300
CO	-14.810634
CO_2	-22.998126
H_2	-6.760199
H_2O	-14.232375
N_2	-16.621003
NO	-12.314807
NO_2	-18.402527
NO_3	-23.374256
O	-1.887207
O_2	-9.877795
OH	-7.744396

Appendix H

Au13 cluster energy vs. box size

To test the effect of the box size on the energy of the system, different cubic cell sizes were used to obtain the energy of the Au_{13} nanoparticle.

box lattice (Å)	Energy (eV)
20	-28.329544
19	-28.329649
18	-28.329209
17	-28.328264
16	-28.32824
15	-28.3283
14	-28.324441
13	-28.317833
12	-28.317833

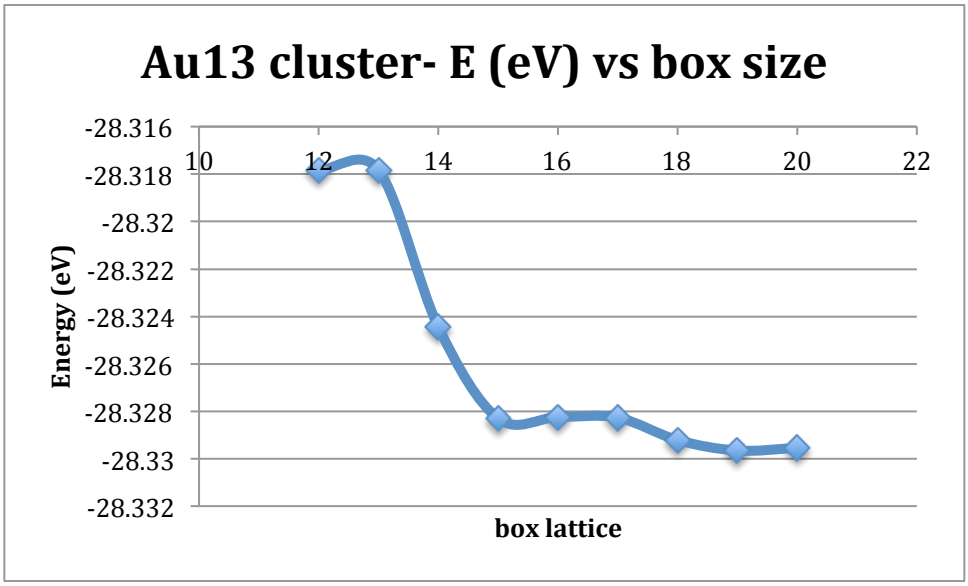

Appendix I

Cubic vs. non-cubic box

To study the effect on the energetics of cubic boxes vs. non-cubic, we calculated reaction energies of NO3 and NO2 reduction on different catalysts on cubic boxes and slightly non-cubic boxes.

Non-Cubic 20.0 Å x 20.2 Å x 20. 4Å			
	Au13	**Au11Fe2**	**Au11FePd**
NO3	-53.377	-61.911	-59.501
NO2	-48.153	-56.481	-54.183
NO2-O	-53.701	-62.074	-59.768
NO-O	-47.289	-57.971	-55.265

Cubic 20.0 Å x 20.0 Å x 20.0 Å			
	Au13	**Au11Fe2**	**Au11FePd**
NO3	-53.340	-61.906	-59.493
NO2	-48.151	-56.480	-54.178
NO2-O	-53.699	-61.548	-59.766
NO-O	-47.287	-57.970	-55.263

	non Cubic	**Cubic**	**Difference**
Au13NO3 → Au13NO2-O	-0.324	-0.359	-0.034
Au13NO2 → Au13NO-O	0.864	0.864	0.000
Au11Fe2NO3→Au11Fe2NO2-O	-0.1624	0.3576	0.5199
Au11Fe2NO2 → Au11Fe2NO-O	-1.4904	-1.4905	-0.0001
Au11FePdNO3 → Au11FePdNO2-O	-0.2669	-0.2736	-0.0067
Au11FePdNO2 →Au11FePdNOO	-1.0823	-1.0852	-0.0029

For the $Au_{11}Fe_2$ case, the difference is very large. The reaction energy for the cubic cell is ~0.5eV higher in energy than the non-cubic. We note that is a strange result and do not know the cause of it.

Appendix J

Charged NO_3^-, NO_2^-, NO^- vs. neutral NO_3, NO_2, NO

To study the effect of having charged molecules vs. neutral molecules, we added an extra electron in the system. To do this, we obtained the number of electrons present in the cell (ZVAL) and added one, then obtained the reaction energies for NO3, NO2 reduction on different catalysts.

	ZVAL (# e-)		NO CHARGE	CHARGED -1
Au	11	**Au13**	143	
N	5	**Au13NO**	154	155
O	6	**Au13NO-O**	160	161
Pd	10	**Au13NO2**	160	161
Fe	8	**Au13NO2-O**	166	167
		Au13NO3	166	167
		Au12Pd	142	
		Au12PdNO	153	154
		Au12PdNO-O	159	160
		Au12PdNO2	159	160
		Au12NO2-O	165	166
		Au12PdNO3	165	166
		Au12Fe	140	
		Au12FeNO	151	152
		Au12FeNO-O	157	158
		Au12FeNO2	157	158
		Au12FeNO2-O	163	164
		Au12FeNO3	163	164

NEUTRAL- NOCHARGE IN BOX			
	Au13	**Au11Fe2**	**Au11FePd**
NO3	-53.340	-61.906	-59.493
NO2	-48.151	-56.480	-54.178
NO2-O	-53.699	-61.548	-59.766
NO-O	-47.287	-57.970	-55.263

NEGATIVE CHARGED -1 IN BOX			
	Au13	**Au11Fe2**	**Au11FePd**
NO3	-56.956	-65.318	-62.963
NO2	-51.545	-59.843	-57.449
NO2-O	-56.964	-65.519	-63.076
NO-O	-50.543	-61.232	-58.341

	neutral	**charged**	**Difference**
Au13NO3 → Au13NO2-O	-0.359	-0.008	-0.351
Au13NO2 → Au13NO-O	0.864	1.001	-0.137

	neutral	charged	Difference
Au11Fe2NO3 → Au11Fe2NO2-O	0.358	-0.200	-0.558
Au11Fe2NO2 → Au11Fe2NO-O	-1.491	-1.388	0.102

	neutral	charged	Difference
Au11FePdNO3 → Au11FePdNO2-O	-0.274	-0.114	0.160
Au11FePdNO2 →Au11FePdNO-O	-1.085	-0.892	0.193

As we notice for the charged systems, the extra charge tends to distribute within the 13 metal atoms in the nanoparticle. When using LDA and GGA exchange functionals, the electrons in the system are allowed to interact with their own charge density; this is very

unrealistic and not physically possible, which causes a raise in the energy of localized states and causes DFT to produce excessively delocalized charge distributions[97]. Therefore, we decided to ignore the extra charge and use the neutral systems. To check whether this approach is correct and verify our methods, DFT+U (with GGA+U exchange functional) or a DFT Hybrid method, such as the Heyd-Scuseria-Ernzerhof (HSE) method could be used[98,99]. These, while a lot more costly, are known to describe the electronic properties of the system better and avoid the self-interaction error.

Bader

	NO3					
	Au13		Au12Pd		Au12Fe	
	neutral	charged	neutral	charged	neutral	charged
Avg. all metal atoms	0.04	-0.02	0.05	-0.02	0.05	-0.02
Avg. coordinated atoms	0.44	0.16	0.53	0.46	0.48	0.33
Doped atom	n.a	n.a	0.30	0.26	0.71	0.76
Adsorbate NOx	-0.58	-0.68	-0.62	-0.69	-0.59	-0.69

	NO2					
	Au13		Au12Pd		Au12Fe	
	neutral	charged	neutral	charged	neutral	charged
Avg all metal atoms	0.03	-0.04	0.04	-0.03	0.03	-0.04
Avg coordinated atoms	0.41	0.30	0.46	0.40	0.38	0.31
Doped atom	n.a	n.a	0.29	0.25	0.81	0.77
Adsorbate NOx	-0.41	-0.52	-0.48	-0.57	-0.43	-0.54

	NO		
	Au13	Au12Pd	Au12Fe

	neutral	charged	neutral	charged	neutral	charged
Avg all metal atoms	0.01	-0.06	0.01	-0.05	0.01	-0.06
Avg coordinated atoms	0.20	0.18	0.43	0.40	0.22	0.21
Doped atom	n.a	n.a	0.43	0.40	0.88	0.79
Adsorbate NOx	-0.11	-0.22	-0.19	-0.30	-0.15	-0.24

Appendix K

Water vs. vacuum environment

An implicit solvation model was used to model the reactions under water environment.

Then the reaction energies were compared on vacuum vs. water environment.

	ext-far			ext-close			center		
	Erxn (vac)	**Erxn (aqu)**	**Δ(vac - aqu)**	**Erxn (vac)**	**Erxn (aqu)**	**Δ(vac - aqu)**	**Erxn (vac)**	**Erxn (aqu)**	**Δ(vac - aqu)**
Au13NO3 → Au13NO2-O	-0.324	-0.092	-0.232						
Au13NO2 → Au13NO-O	0.864	0.788	0.076						
Au12FeNO3 → Au12FeNO2-O	-0.13	-0.139	0.009	0.067	-0.058	0.125	0.046	0.013	0.033
Au12FeNO2 →Au12FeNO-O	-0.301	0.017	-0.318	-0.101	-0.075	-0.026	1.119	1.029	0.09
Au12PdNO3 → Au12dNO2-O	0.037	-0.075	0.112	-0.109	-0.206	0.097	-0.097	-0.212	0.115
Au12PdNO2 → Au12NO-O	0.711	0.711	0.00	0.127	0.15	-0.023	0.94	0.828	0.112
Au12CuNO3 →Au12CuNO2-O	-0.2	-0.177	-0.023	-0.063	-0.035	-0.028	-0.407	-0.404	-0.003
Au12CuNO2 → Au12CuNO-O	0.328	0.278	0.05	1.122	1.102	0.02	0.843	0.742	0.101
Au12InNO3 → Au12InNO2- O	-0.184	-0.151	-0.033	0.418	0.291	0.127	-0.203	-0.122	-0.081
Au12InNO2 → Au12INNO-O	1.256	1.775	-0.519	1.57	1.562	0.008	1.5	1.42	0.08
Au11Fe2NO3 → Au11Fe2NO2-O	-0.162	-0.084	-0.078						
Au11Fe2NO2 → Au11Fe2NO-O	-1.49	-0.998	-0.492						
Au11FePdNO3→Au11FePdNO2-O	-0.267	-0.335	0.068						
Au11FePdNO2→Au11FePdNO-O	-1.082	-0.808	-0.274						
Au11Pd2NO3 →Au11Pd2NO2-O	-0.131	-0.214	0.083						
Au11Pd2NO2→Au11Pd2NO-O	0.394	0.393	0.001						

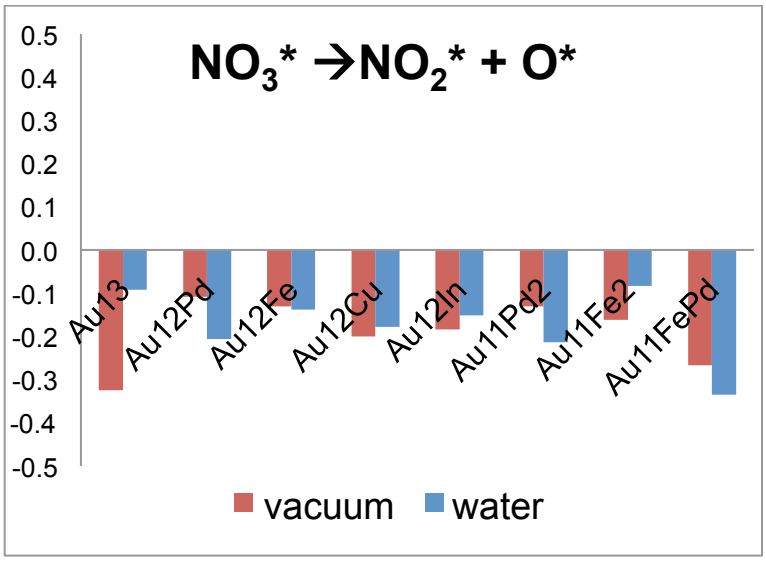
NO3* →NO2* + O*
0.5
0.4
0.3
0.2
0.1
0.0
-0.1
-0.2
-0.3
-0.4
-0.5
Au13
Au12Pd
Au12Fe
Au12Cu
Au12In
Au11Pd2
Au11Fe2
Au11FePd
vacuum
water

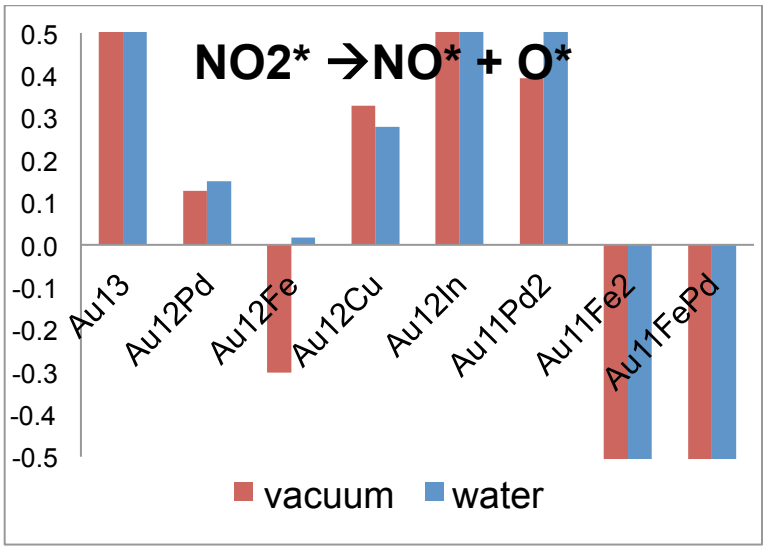
NO2* →NO* + O*
0.5
0.4
0.3
0.2
0.1
0.0
-0.1
-0.2
-0.3
-0.4
-0.5
Au13
Au12Pd
Au12Fe
Au12Cu
Au12In
Au11Pd2
Au11Fe2
Au11FePd
vacuum
water

Appendix L

Bader for all systems

To study the distribution of charge in the system, the partial charge of the atoms was calculated using Henkelman's algorithm for Bader charge analysis. X,Y can be Au, Pd, or Fe atoms depending on each case.

NO_3

Atom	Au13	Au12Pd	Au12Fe	Au11Fe2	Au11FePd	Au11Pd2
1	0.019	-0.009	-0.020	-0.195	-0.172	0.032
2	-0.029	-0.068	-0.134	0.243	-0.118	-0.055
3	0.198	0.012	-0.169	-0.145	-0.177	-0.078
4	0.247	0.002	-0.055	0.196	-0.072	0.004
5	-0.024	0.019	0.209	-0.210	0.013	0.016
6	-0.019	-0.018	-0.023	-0.027	-0.199	-0.008
7	0.049	0.021	-0.153	-0.176	0.198	-0.076
8	-0.021	-0.008	-0.025	0.068	0.106	0.179
9	-0.001	0.195	0.149	-0.064	0.046	0.070
10	0.195	0.237	-0.209	-0.286	-0.276	-0.108
11	-0.026	-0.053	0.266	-0.070	-0.060	0.080
Y	-0.029	-0.010	-0.042	0.616	0.926	0.292
X	0.018	0.296	0.799	0.667	0.371	0.289
NO3 adsorbate	**-0.576**	**-0.616**	**-0.590**	**-0.618**	**-0.585**	**-0.637**

NO_2

Atom	Au13	Au12Pd	Au12Fe	Au11Fe2	Au11FePd	Au11Pd2
1	0.020	0.020	-0.029	-0.232	-0.182	0.012
2	-0.040	-0.072	-0.197	-0.087	-0.048	-0.054
3	-0.072	0.016	-0.183	-0.148	-0.193	-0.078
4	0.023	-0.016	0.206	0.162	-0.092	-0.004
5	-0.070	-0.011	-0.040	-0.206	-0.012	-0.006
6	-0.051	-0.009	0.171	0.224	-0.188	-0.007
7	0.043	-0.022	-0.226	-0.156	0.192	-0.076
8	-0.071	-0.020	-0.039	0.068	0.107	0.184
9	-0.040	0.191	0.150	-0.034	0.018	0.050
10	0.283	0.174	-0.178	-0.335	-0.213	-0.097

11	0.174	-0.062	-0.010	-0.085	-0.038	0.052
Y	-0.024	0.008	-0.008	0.652	0.813	0.277
X	0.240	0.288	0.818	0.634	0.300	0.288
NO2 adsorbate	**-0.414**	**-0.485**	**-0.433**	**-0.458**	**-0.463**	**-0.540**

NO

Atom	Au13	Au12Pd	Au12Fe	Au11Fe2	Au11FePd	Au11Pd2
1	-0.023	0.009	-0.027	-0.214	-0.213	-0.107
2	0.197	-0.077	-0.152	-0.083	-0.076	-0.047
3	0.015	-0.069	-0.151	-0.165	-0.149	-0.066
4	-0.054	-0.043	-0.026	0.012	-0.066	-0.008
5	-0.040	-0.053	-0.016	-0.261	-0.052	-0.081
6	-0.051	0.032	0.209	0.312	-0.213	0.042
7	-0.035	-0.079	-0.192	-0.164	-0.074	-0.064
8	-0.011	-0.049	-0.043	0.048	0.078	0.128
9	0.016	0.184	0.123	-0.113	-0.082	-0.012
10	0.195	-0.075	-0.194	-0.348	-0.150	-0.124
11	-0.017	-0.051	-0.033	-0.083	-0.064	-0.018
Y	-0.036	0.025	-0.036	0.612	0.803	0.115
X	-0.048	-0.975	0.687	0.632	0.427	0.429
NO adsorbate	**-0.108**	**-0.187**	**-0.149**	**-0.185**	**-0.170**	**-0.187**

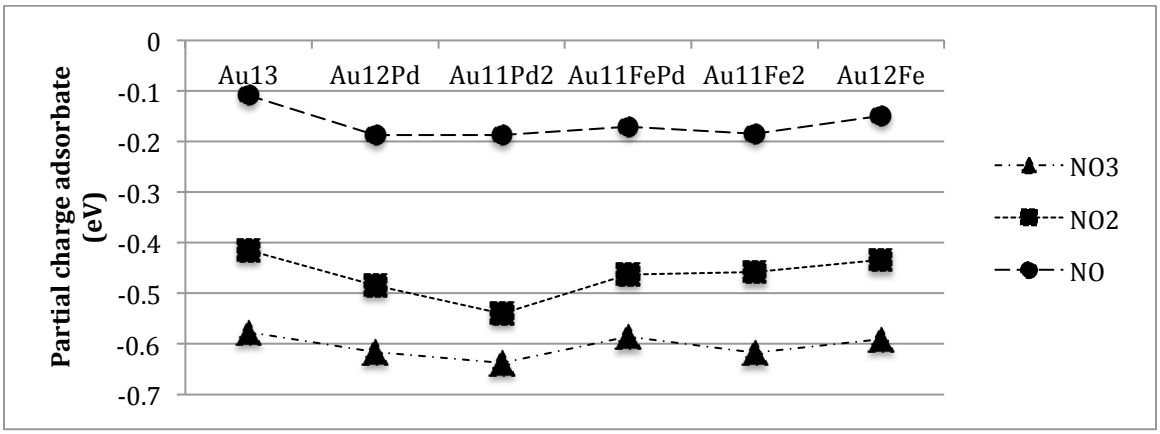

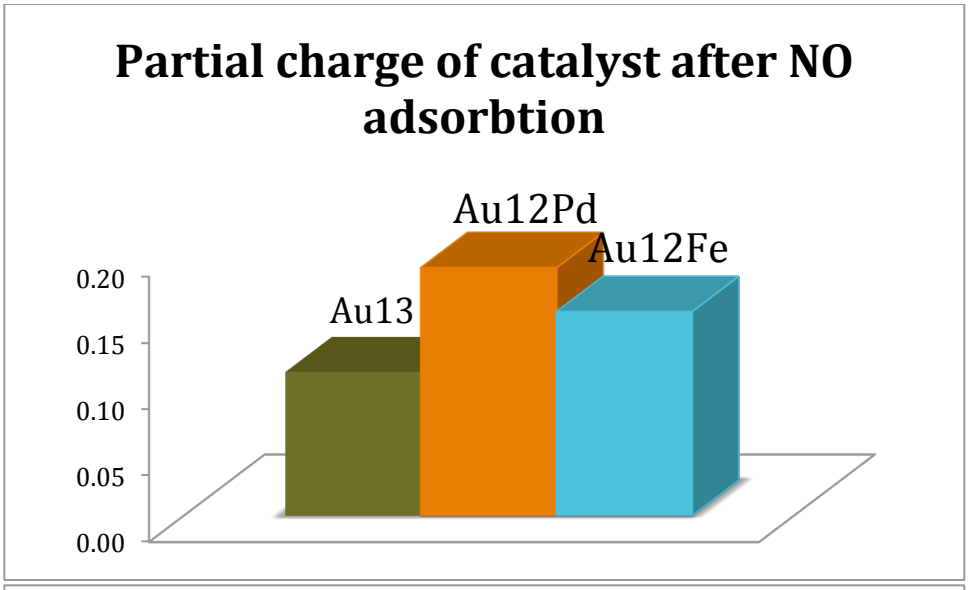
Partial charge of catalyst after NO adsorbtion
Au13
Au12Pd
Au12Fe
0.20
0.15
0.10
0.05
0.00

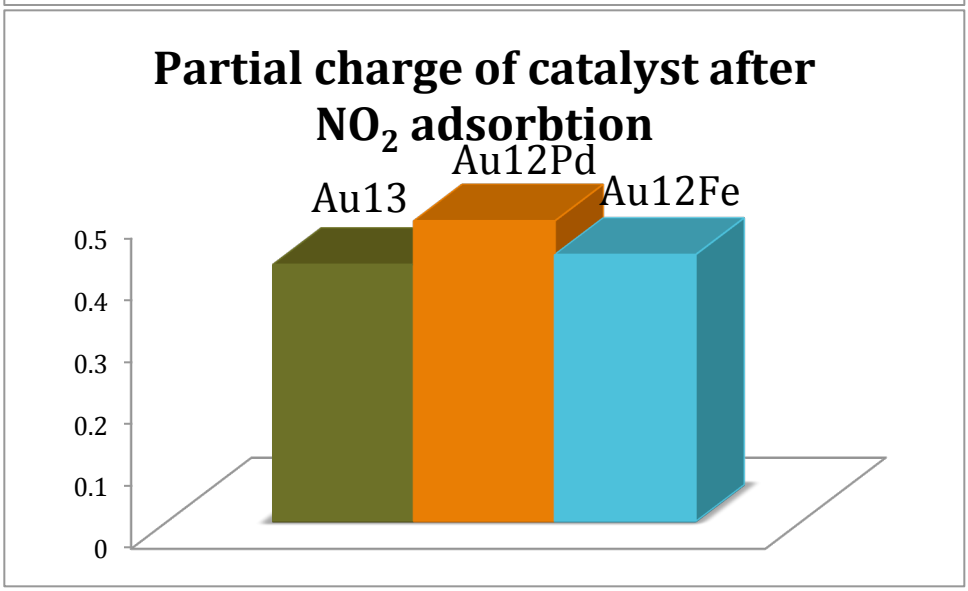
Partial charge of catalyst after NO_2 adsorbtion
Au13
Au12Pd
Au12Fe
0.5
0.4
0.3
0.2
0.1
0

Appendix M

Density Of States (DOS)

DOS NO

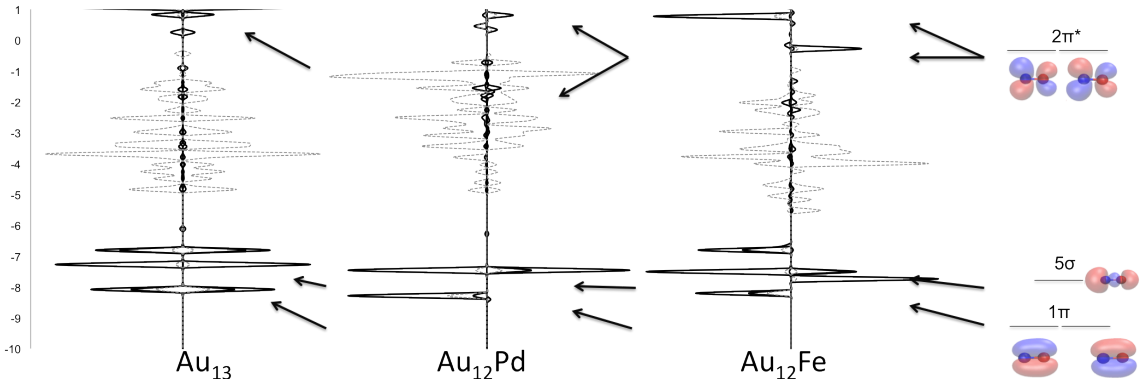

DOS NO_2

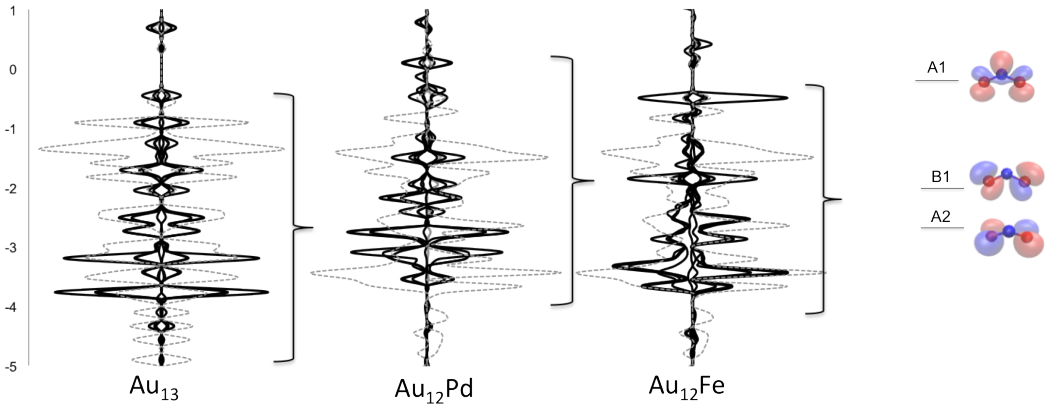

Appendix N

Material Properties

Using the dissociation energies of the most favorable compositions, we tried to find a correlation to a material property. We computed d band center of the bulk X metal, d band center of the bare 13-atom nanoparticle. We also studied 3 different molecules as adsorbates on the different catalysts: NO_3, NO_2 and NO. We used the adsorption energies, the d band center of the nanoparticle with an adsorbate and the metal-adsorbate distance. Table X summarized this data.

We then proceeded to find correlations between the different reaction energies and the different materials properties depending on the position of the X atom.

Table N-1. Table summarizing different material properties for each catalyst.

	Au13	**Au12Pd**			**Au12Fe**			**Au12Cu**			**Au12In**		
		C	EC	EF	C	EC	EF	C	EC	EF	C	EC	EF
d band center bulk X metal	-2.84	-1.56			-1.10			-1.81			-8.24		
d band center bare nanoparticle	-1.94	-1.95	-1.95		-2.19	-2.13		-1.74	-1.96		-2.28	-2.93	
NO3													
E ads (eV)	-1.67	-1.93	-1.83	-1.69	-1.50	-2.58	-1.63	-1.64	-2.19	-1.64	-1.87	-1.84	-1.39
d band center metal within adsorption	-2.84	-2.70	-2.79	-2.76	-3.02	-2.92	1.45	-2.71	-2.80	-2.83	-2.96	-2.99	-2.90
metal-adsorbate distance (Å)	2.23	2.19	2.16	2.20	2.22	2.24	2.21	2.21	2.18	2.29	2.27	2.31	2.31
NO2													
E ads (eV)	-1.42	-1.47	-1.42	-1.13	-1.13	-1.89	-1.14	-1.48	-1.76	-1.33	-1.68	-0.91	-0.97
d band center metal within adsorption	-2.67	-2.70	1.50	-2.61	-2.82	-2.70	-2.78	-2.59	1.76	-2.69	-2.81	-2.63	-2.78
metal-adsorbate distance (Å)	2.22	2.23	2.19	2.23	2.23	2.13	2.23	2.24	2.11	2.24	2.21	2.47	2.31
NO													
E ads (eV)	-1.16	-1.19	-1.75	-0.63	-0.91	-2.60	-0.83	-1.26	-1.27	-1.10	-0.82	-0.16	-0.02
d band center metal within adsorption	-2.54	-2.51	-2.49	1.72	-2.77	-2.59	-2.78	-2.46	-2.62	-2.58	-2.84	-2.76	-2.78
metal-adsorbate distance (Å)	2.02	2.03	1.82	2.04	2.01	1.65	2.03	2.03	1.83	2.03	2.07	2.57	1.99

Appendix O

Correlation to material properties

Using the dissociation energies of the most favorable compositions, we tried to find a correlation to a material property. We computed d band center of the bulk X metal, and the d band center of the bare 13-atom nanoparticle. We also studied 3 different molecules as adsorbates on the different catalysts: NO_3, NO_2 and NO to obtain adsorption energies, the d band center of the nanoparticle with the adsorbate, and the metal-adsorbate distance as possible descriptors of NO_2 reduction activity. Table N-1 on appendix N summarizes the different material properties for each catalyst.

We then proceeded to find correlations between the different reaction energies and the different materials properties depending on the position of the X atom. Exterior Close (EC) and Center (C)

Fig. O-1 shows when the alloying X atom is found at the center (C) or at the exterior-close position (EC) the dissociating energy of NO_2 is directly correlated to the adsorption energy of NO to the nanoparticle. The stronger the adsorption (lower Eads) of NO, the lower is the reaction energy for NO_2. The product (NO) is bound more strongly to the catalyst when the adsorption energy is lower, so reaction will favor production of NO resulting in lower reaction energies. When the atom is placed at C or EC position, it is still close to the adsorbate, so it's understandable that the ability to create a strong chemisorption with the products of the reaction is a good parameter to measure for reaction energies.

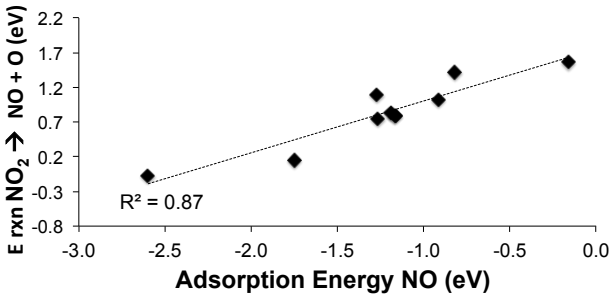

Figure O-1 EC and C energies vs. adsorption energy for NO molecule. The data shows a linear correlation.

Since we found that the ability to strongly adsorb NO correlates to favorable thermodynamics for NO_2 dissociation, we then tried to find the cause of the adsorption energy for the C and EC separately.

Fig. O-2 shows that for the EC case, the adsorption energy, linearly correlates to the bond distance between the metal and the NO. The smaller the distance, the lower the adsorption energy. When the bond is stronger, the distance between the metal and the adsorbate will be shorter and the adsorption energy will be low

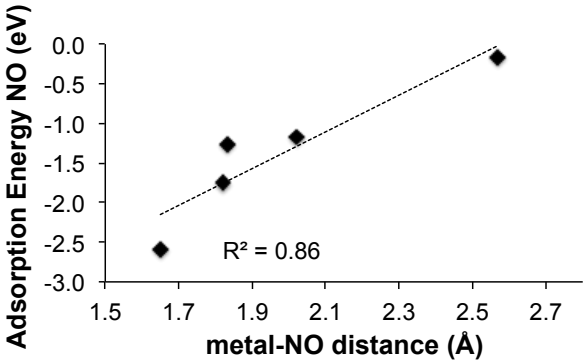

Fig. O-2 Linear correlation between adsorption energy of NO and metal-NO bond distance for EC case

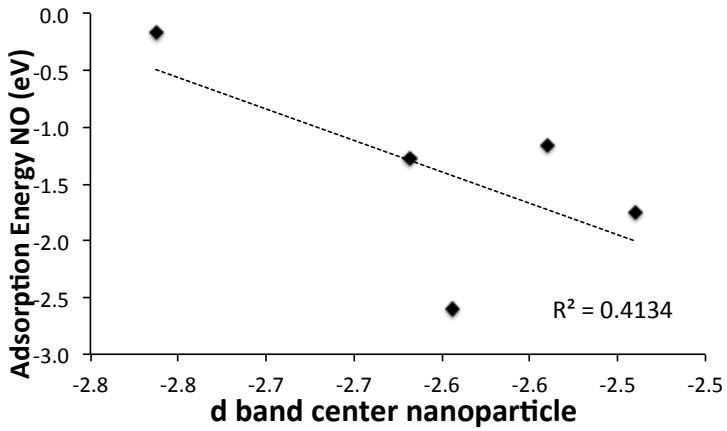

Fig O-3 No correlation between adsorption energy of NO and d band center of the nanoparticle for EC case

For when X is at the center, we did not see the same trends as for the exterior-close case. Fig O-3 shows that for this case, the adsorption energy linearly correlates to the d band center of the nanoparticle.

Since the alloying X atom is not in direct contact with the adsorbate, we cannot use the metal-adsorbate distance as parameter. As we mentioned before, the d band center of a metal is also a good measurement to its ability to create stronger bonds. When the d band center is higher, the adsorption energy is stronger.

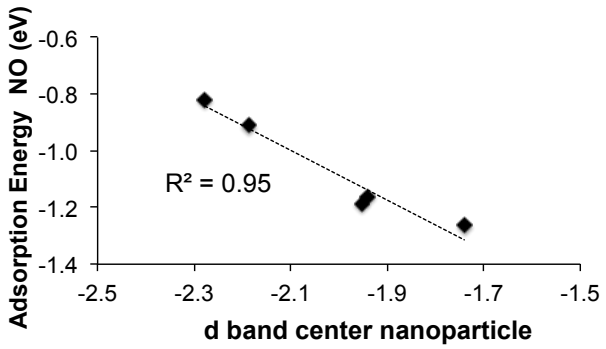

Fig O-4 Linear correlation between adsorption energy of NO and d band center of the nanoparticle for the C case

Exterior Far (EF)

For the case when the alloying atom is in the exterior and the furthest from the adsorbates, the exterior far (EF) case, we found that none of the parameters that correlate for the EC and C case, correlated here. It's actually the charge of the X atom within NO adsorption, the one that linearly correlates to the dissociation energy of NO_2. When the charge is higher, the reaction energy is lower. This tells us that the alloying metal plays a big role even when it's the furthest from the adsorbates by giving charge to allow back donation of electrons. We found that for X=In, it did not fit the trend. The charge of In was negative within NO adsorption and the charge of the adsorbate NO was positive, indicating that the charge was going from NO to the nanoparticle. Therefore, it was not included in the plot.

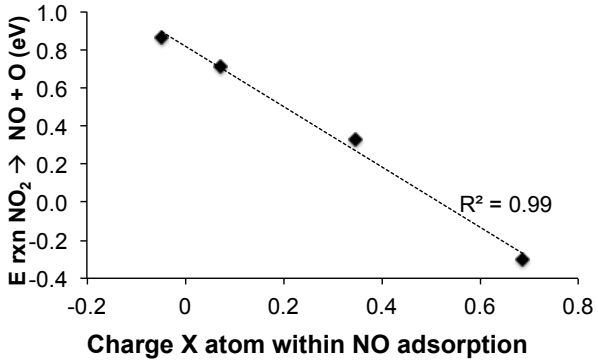

Figure O-5 EF energies vs. charge X atom when NO molecule is adsorbed. The plot shows a linear correlation. Partial charge was calculated suing Bader algorithm for Henkelman charge analysis

REFERENCES

1. Watkins K, Carvajal L, Coppard D, Fuentes R, Ghosh A, Giamberardini C. *Human development report 2006: Beyond scarcity: Power, poverty and the global water crisis.* United Nations Development Programme (UNDP); 2006.

2. Department of Agriculture US. Irrigation and water use. http://www.ers.usda.gov/topics/farm-practices-management/irrigation-water-use.aspx#.Uyemuxb_dG5. Updated 2013. Accessed March/02, 204.

3. Centi G, Perathoner S. Remediation of water contamination using catalytic technologies. *Applied Catalysis B: Environmental*. 2003;41(1):15-29.

4. Matatov-Meytal YI, Sheintuch M. Catalytic abatement of water pollutants. *Ind Eng Chem Res*. 1998;37(2):309-326.

5. Environmental Protection Agency US. Our water: Tomorrow & beyond. http://www.epa.gov/watersense/our_water/tomorrow_beyond.html. Updated 2014. Accessed February/10, 2014.

6. United Nations. Water: A shared responsibility. the united nations world water development report 2. 2006. http://www.unesco.org/bpi/wwap/press/. Updated 2006. Accessed March/01, 2014.

7. Environmental Protection Agency, United States. Primer for municipal wastewater treatment systems. http://www.epa.gov/npdes/pubs/primer.pdf. Updated 2004. Accessed February/10, 2014.

8. Schwarzenbach RP, Escher BI, Fenner K, et al. The challenge of micropollutants in aquatic systems. *Science*. 2006;313(5790):1072-1077. doi: 10.1126/science.1127291.

9. Westerhoff P, Yoon Y, Snyder S, Wert E. Fate of endocrine-disruptor, pharmaceutical, and personal care product chemicals during simulated drinking water treatment processes. *Environ Sci Technol*. 2005;39(17):6649-6663.

10. Benotti MJ, Trenholm RA, Vanderford BJ, Holady JC, Stanford BD, Snyder SA. Pharmaceuticals and endocrine disrupting compounds in US drinking water. *Environ Sci Technol*. 2008;43(3):597-603.

11. Environmental Protection Agency US. National primary drinking water regulations. http://water.epa.gov/drink/contaminants/upload/mcl-2.pdf. Accessed February/10, 2014.

12. Davis ML, Cornwell DA. *Introduction to environmental engineering.* Vol 3. McGraw-Hill New York; 1998.

13. Open University of Tanzania. Nature and types of Water pollutants. http://www.out.ac.tz/avu/images/Chemistry/11_Environmental%20Chemistry/env_comp_readings_20080911/Comp-R-waterpollutants-andWHO%20guideline.pdf. Updated 2008. Accessed 15/01, 2014.

14. Environmental Protection Agency US. What is nonpoint source pollution? http://water.epa.gov/polwaste/nps/whatis.cfm. Updated 2012. Accessed March/01, 2014.

15. National Ocean Service Education. Nonpoint sources of pollution. http://oceanservice.noaa.gov/education/kits/pollution/04nonpointsource.html. Updated 2008. Accessed March/12, 2014.

16. Davis ML. *Water and wastewater engineering*. McGraw-Hill New York; 2010.

17. Denver Water. The water treatment process. http://www.denverwater.org/WaterQuality/TreatmentProcess/. Updated 2014. Accessed March/03, 2014.

18. Wikipedia. Wastewater treatment process. http://en.wikipedia.org/wiki/Sewage_treatment. Accessed February/12, 2014.

19. Wells MJ, Fono LJ, Pellegrin M, Morse A. Emerging pollutants. *Water Environ Res*. 2007;79(10):2192-2209.

20. Gates BC, Katzer JR, Schuit GC. *Chemistry of catalytic processes.* Vol 464. McGraw-Hill New York; 1979.

21. Spalding RF, Exner ME. Occurrence of nitrate in groundwater—a review. *J Environ Qual*. 1993;22(3):392-402.

22. Robarts R. United nations environment programme global environment monitoring system (GEMS)/water programme: state of water quality assessment reporting at the global level. presentation at the UN international work session on water statistics. http://unstats.un.org/unsd/environment/watersess_papers.htm. Updated 2004. Accessed March/05, 2014.

23. Curry S. Methemoglobinemia. *Ann Emerg Med*. 1982;11(4):214-221.

24. National Library of Medicine, U.S. Methemoglobinemia. http://www.ncbi.nlm.nih.gov/pubmedhealth/PMH0001588/. Updated 2013. Accessed February/12, 2014.

25. Art HW. *Dictionary of ecology and environmental science*. 1993.

26. Louisiana Universities Marine Consortium. Hypoxia in the northern gulf of mexico. http://www.gulfhypoxia.net/overview/. Accessed 01/20, 2014.

27. Kapoor A, Viraraghavan T. Nitrate removal from drinking water-review. *J Environ Eng*. 1997;123(4):371-380.

28. Richard Y, Leprince A, Martin G, Leblanc C. Denitrification of water for human consumption. *Progress in Water Technology*. 1980;12.

29. Hörold S, Vorlop K, Tacke T, Sell M. Development of catalysts for a selective nitrate and nitrite removal from drinking water. *Catalysis Today*. 1993;17(1):21-30.

30. Vorlop K, Prusse U, Janssen F, van Santen R. Catalytical removing nitrate from water. *Catalytic science series*. 1999;1:195-218.

31. Prüsse U, Hähnlein M, Daum J, Vorlop K. Improving the catalytic nitrate reduction. *Catalysis Today*. 2000;55(1):79-90.

32. Gauthard F, Epron F, Barbier J. Palladium and platinum-based catalysts in the catalytic reduction of nitrate in water: Effect of copper, silver, or gold addition. *Journal of Catalysis*. 2003;220(1):182-191.

33. Mikami I, Sakamoto Y, Yoshinaga Y, Okuhara T. Kinetic and adsorption studies on the hydrogenation of nitrate and nitrite in water using pd-cu on active carbon support. *Applied Catalysis B: Environmental*. 2003;44(1):79-86.

34. Mikami I, Yoshinaga Y, Okuhara T. Rapid removal of nitrate in water by hydrogenation to ammonia with zr-modified porous ni catalysts. *Applied Catalysis B: Environmental*. 2004;49(3):173-179.

35. Soares OSG, Órfão JJ, Pereira MFR. Activated carbon supported metal catalysts for nitrate and nitrite reduction in water. *Catalysis letters*. 2008;126(3-4):253-260.

36. Marchesini F, Irusta S, Querini C, Miró E. Nitrate hydrogenation over pt, in/al< sub> 2 O< sub> 3 and pt, in/SiO< sub> 2. effect of aqueous media and catalyst surface properties upon the catalytic activity. *Catalysis Communications*. 2008;9(6):1021-1026.

37. Calvo L, Gilarranz MA, Casas JA, Mohedano AF, Rodriguez JJ. Denitrification of water with activated carbon-supported metallic catalysts. *Ind Eng Chem Res*. 2010;49(12):5603-5609.

38. Gavagnin R, Biasetto L, Pinna F, Strukul G. Nitrate removal in drinking waters: The effect of tin oxides in the catalytic hydrogenation of nitrate by pd/SnO_2 catalysts. *Applied Catalysis B: Environmental*. 2002;38(2):91-99.

39. Wong MS, Alvarez PJ, Fang Y, et al. Cleaner water using bimetallic nanoparticle catalysts. *Journal of chemical technology and biotechnology*. 2009;84(2):158-166.

40. Oura K, Lifshits V, Saranin A, Zotov A, Katayama M. Hydrogen interaction with clean and modified silicon surfaces. *Surface science reports*. 1999;35(1):1-69.

41. Eliassen R, Tchobanoglous G. Removal of nitrogen and phosphorus from waste water. *Environ Sci Technol*. 1969;3(6):536-541

42. Samatya S, Kabay N, Yüksel Ü, Arda M, Yüksel M. Removal of nitrate from aqueous solution by nitrate selective ion exchange resins. *React Funct Polym*. 2006;66(11):1206-1214.

43. Philipot J, De Larminat G. Nitrate removal by ion exchange: The ECODENIT process, an industrial scale facility at binic(france). *Water Supply*. 1988;6(3):45-50.

44. The Water Planet Company. Nitrogen removal from wastewater: Nitrogen chemistry. http://www.cleanwaterops.com/wp-content/uploads/2014/01/Clean-Water-Ops-_-White-Paper_Nitrogen-Chemistry.pdf. Updated 2014. Accessed 03/02, 2014.

45. Tanabe K, Shapiro B. Heterogeneous catalysis. *Texas A and M University Press, College Station, TX*. 1984:71.

46. Lindström B, Pettersson LJ. A brief history of catalysis. *CatTech*. 2003;7(4):130-138.

47. Thomas JM, Thomas WJ, Salzberg H. Introduction to the principles of heterogeneous catalysis. *J Electrochem Soc*. 1967;114(11):279C-279C.

48. Cornils B, Herrmann WA, Muhler M, Wong C. C*atalysis from A to Z*. Wiley-VCH Weinheim,Germany. 2008.

49. Bond GC. *Heterogeneous catalysis*: principles and aplications. Clarendon Press. Oxford .1974.

50. North Carolina School of Science and Mathematics. Potential energy diagram for a catalyzed and uncatalyzed multi-step reaction. http://www.dlt.ncssm.edu/tiger/chem5.htm. Updated 2014. Accessed March/05, 2014.

51. White MG. *Heterogeneous catalysis.* Prentice Hall Upper Saddle River, NJ, USA; 1990.

52. Sabatier P. *Catalysis in organic chemistry.* D. Van Nostrand Company; 1922.

53. University of California, Santa Barbara. Ab initio and electronic structure methods. http://www.engr.ucsb.edu/~shell/che210d/Ab_Initio_methods.pdf. Updated 2014. Accessed 03/01, 2014.

54. Time–Independent schrödinger equation. http://homepage.univie.ac.at/reinhold.bertlmann/pdfs/T2_Skript_Ch_4.pdf. Accessed 03/02, 2014.

55. Kresse G, Hafner J. Ab initio molecular dynamics for liquid metals. *Physical Review B*. 1993;47(1):558.

56. Kresse G, Hafner J. Ab initio molecular-dynamics simulation of the liquid-metal–amorphous-semiconductor transition in germanium. *Physical Review B*. 1994;49(20):14251.

57. Kresse G, Furthmüller J. Efficiency of ab-initio total energy calculations for metals and semiconductors using a plane-wave basis set. *Computational Materials Science*. 1996;6(1):15-50.

58. Kresse G, Furthmüller J. Efficient iterative schemes for ab initio total-energy calculations using a plane-wave basis set. *Physical Review B*. 1996;54(16):11169.

59. Perdew JP, Zunger A. Self-interaction correction to density-functional approximations for many-electron systems. *Physical Review B*. 1981;23(10):5048.

60. Durham University. Generalized gradient approximations. http://cmt.dur.ac.uk/sjc/thesis_dlc/node30.html. Updated 2003. Accessed 01/29, 2014.

61. Perdew JP, Chevary J, Vosko S, et al. Atoms, molecules, solids, and surfaces: Applications of the generalized gradient approximation for exchange and correlation. *Physical Review B*. 1992;46(11):6671.

62. Perdew JP, Burke K, Ernzerhof M. Generalized gradient approximation made simple. *Phys Rev Lett*. 1996;77(18):3865.

63. Bylaska EJ. Introduction to plane-wave basis sets and pseudopotential theory**.** http://www.nwchem-sw.org/images/Pw-lecture.pdf. Accessed February/03, 2014.

64. Kresse G. Pseudopotentials (part I) https://www.vasp.at/vasp-workshop/slides/pseudopp1.pdf. Accessed March/01, 2014.

65. Haynes PD. Linear-scaling methods in ab initio quantum-mechanical calculations. http://www.tcm.phy.cam.ac.uk/~pdh1001/thesis/thesis.html. Updated 1998. Accessed 01/29, 2014.

66. The Shodor Education Foundation, Inc. Glossary for computational chemistry. https://www.shodor.org/chemviz/glossary.html. Updated 200. Accessed March/02, 2014.

67. Mennucci B. Polarizable continuum model. *Wiley Interdisciplinary Reviews: Computational Molecular Science*. 2012;2(3):386-404.

68. Tomasi J, Mennucci B, Cammi R. Quantum mechanical continuum solvation models. *Chem Rev*. 2005;105(8):2999-3094.

69. Norskov JK, Abild-Pedersen F, Studt F, Bligaard T. Density functional theory in surface chemistry and catalysis. *Proc Natl Acad Sci U S A*. 2011;108(3):937-943. doi: 10.1073/pnas.1006652108; 10.1073/pnas.1006652108.

70. Asthagiri A, Janik M. *Computational catalysis.* Vol 14. Royal Society of Chemistry; 2013.

71. Kitchin J, Nørskov JK, Barteau M, Chen J. Modification of the surface electronic and chemical properties of pt (111) by subsurface 3d transition metals. *J Chem Phys*. 2004;120(21):10240-10246.

72. Hammer B, Nørskov JK. Theoretical surface science and catalysis—calculations and concepts. *Advances in catalysis*. 2000;45:71-129.

73. Hammer B, Scheffler M. Local chemical reactivity of a metal alloy surface. *Phys Rev Lett*. 1995;74(17):3487.

74. Singh J, Nelson RC, Vicente BC, Scott SL, van Bokhoven JA. Electronic structure of alumina-supported monometallic pt and bimetallic PtSn catalysts under hydrogen and carbon monoxide environment. *Physical Chemistry Chemical Physics*. 2010;12(21):5668-5677.

75. Hammer B, Morikawa Y, Nørskov JK. CO chemisorption at metal surfaces and overlayers. *Phys Rev Lett*. 1996;76(12):2141.

76. Henkelman G, Arnaldsson A, Jónsson H. A fast and robust algorithm for bader decomposition of charge density. *Computational Materials Science*. 2006;36(3):354-360.

77. Tang W, Sanville E, Henkelman G. A grid-based bader analysis algorithm without lattice bias. *Journal of Physics: Condensed Matter*. 2009;21(8):084204.

78. Sanville E, Kenny SD, Smith R, Henkelman G. Improved grid-based algorithm for bader charge allocation. *Journal of computational chemistry*. 2007;28(5):899-908.

79. Assadollahzadeh B, Schwerdtfeger P. A systematic search for minimum structures of small gold clusters aun (n= 2–20) and their electronic properties. *J Chem Phys*. 2009;131(6):064306.

80. Sardar R, Funston AM, Mulvaney P, Murray RW. Gold nanoparticles: Past, present, and future†. *Langmuir*. 2009;25(24):13840-13851.

81. Ketchie WC, Fang Y, Wong MS, Murayama M, Davis RJ. Influence of gold particle size on the aqueous-phase oxidation of carbon monoxide and glycerol. *Journal of catalysis*. 2007;250(1):94-101.

82. Haruta M. Size-and support-dependency in the catalysis of gold. *Catalysis Today*. 1997;36(1):153-166.

83. Ketchie WC, Murayama M, Davis RJ. Promotional effect of hydroxyl on the aqueous phase oxidation of carbon monoxide and glycerol over supported au catalysts. *Topics in Catalysis*. 2007;44(1-2):307-317.

84. Bar-Ilan O, Albrecht RM, Fako VE, Furgeson DY. Toxicity assessments of multisized gold and silver nanoparticles in zebrafish embryos. *Small*. 2009;5(16):1897-1910.

85. He M. A computational approach for the rational design of bimetallic clusters for ethanol formation from syn-gas. . 2013.

86. Villars P, Cenzual K. Pearson's crystal data, crystal structure database for inorganic compounds. *Materials Park (OH): ASM International*. 2007.

87. Doye JP, Meyer L. Mapping the magic numbers in binary lennard-jones clusters. *Phys Rev Lett*. 2005;95(6):063401.

88. Molayem M, Grigoryan VG, Springborg M. Theoretical determination of the most stable structures of niag bimetallic nanoalloys. *The Journal of Physical Chemistry C*. 2011;115(15):7179-7192.

89. Frisch M, Trucks G, Schlegel H, et al. Gaussian 09, revision A. 1. wallingford CT: Gaussian. *Inc OpenURL*. 2009.

90. Jansen APJ. The chemical bond. http://chembond.catalysis.nl/ChemBond/notes/lcao/lcao.html. Updated 2003. Accessed February/20, 2014.

91. Blöchl PE. Projector augmented-wave method. *Physical Review B*. 1994;50(24):17953.

92. Kresse G, Joubert D. From ultrasoft pseudopotentials to the projector augmented-wave method. *Physical Review B*. 1999;59(3):1758.

93. Faheem M, Suthirakun S, Heyden A. New implicit solvation scheme for solid surfaces. *The Journal of Physical Chemistry C*. 2012;116(42):22458-22462.

94. Krishnan R, Binkley JS, Seeger R, Pople JA. Self-consistent molecular orbital methods. XX. A basis set for correlated wave functions. *J Chem Phys*. 2008;72(1):650-654.

95. Hay PJ, Wadt WR. Ab initio effective core potentials for molecular calculations. potentials for the transition metal atoms sc to hg. *J Chem Phys*. 1985;82(1):270-283.

96. McCarthy M, Rosmus P, Werner H, Botschwina P, Vaida V. Dissociation of NH3 to NH2 H. *J Chem Phys*. 1987;86(12):6693-6700.

97. Cramer CJ, Truhlar DG. Density functional theory for transition metals and transition metal chemistry. *Physical Chemistry Chemical Physics*. 2009;11(46):10757-10816.

98. Anisimov VI, Zaanen J, Andersen OK. Band theory and mott insulators: Hubbard U instead of stoner I. *Physical Review B*. 1991;44(3):943.

99. Heyd J, Scuseria GE, Ernzerhof M. Hybrid functionals based on a screened coulomb potential. *J Chem Phys*. 2003;118(18):8207-8215.